Meteoritics & Planetary Science 35, 651–666 (2000)

Numbers, types, and compositions of an unbiased collection of cosmic spherules

SUSAN TAYLOR[1]*, JAMES H. LEVER[1] AND RALPH P. HARVEY[2]

[1]U.S. Army Cold Regions Research and Engineering Laboratory, Hanover, New Hampshire 03755, USA
[2]Case Western Reserve University, Cleveland, Ohio 44106, USA
*Correspondence author's e-mail address: staylor@crrel.usace.army.mil

(Received 1999 June 10; accepted in revised form 2000 January 5)

Abstract–Micrometeorites collected from the bottom of the South Pole water well (SPWW) may represent a complete, well-preserved sample of the cosmic dust that accreted on Earth from 1100–1500 A.D. We classified 1588 cosmic spherules in the size range 50–800 μm. The collection has 41% barred olivine spherules, 17% glass spheres, 12% cryptocrystalline spherules, 11% porphyritic olivine spherules, 12% relic-grain-bearing spherules, 3% scoriaceous spherules, 2% I-type spherules, 1% Ca-Al-Ti-rich (CAT) spherules, and 1% G-type spherules. We also found bubbly glass spherules, spherules with glass caps, and ones with sulfide coatings—particles that are absent from other collections. A classification sequence of the stony spherules (scoriaceous, relic-grain-bearing, porphyritic, barred olivine, cryptocrystalline, glass, and CAT) is consistent with progressive heating and evaporation of Fe from chondritic materials. The modern-day accretion rate and size distribution measured at the SPWW can account for the stony spherules present in deep-sea collection through preferential dissolution of glass and small stony spherules. However, weathering alone cannot account for the high accretion rate of I-type spherules determined for two deep-sea collections. The SPWW collection provides data to constrain models of atmospheric-entry heating and to assess the effects of terrestrial weathering.

INTRODUCTION

Micrometeorites are terrestrially collected extraterrestrial particles smaller than ~1 mm. They range from irregularly shaped unmelted particles to spheroidal, partially to wholly melted "cosmic spherules". These materials contribute most of the mass accreted to the present-day Earth (Peucker-Ehrenbrink, 1996; Love and Brownlee, 1993; Brownlee, 1981), and large collections should contain samples of asteroids, the Moon, Mars, and cometary materials not represented in meteorite collections (Bradley *et al.*, 1988; Brownlee *et al.*, 1993). Estimates on the amount of this material entering the Earth's upper atmosphere vary, with accepted values close to 30 000 ton year^{-1} (Love and Brownlee, 1993; Peucker-Ehrenbrink and Ravizza, 2000). Because of the large number of micrometeorites arriving on Earth, rare or unusual extraterrestrial materials are more likely to be found in micrometeorite rather than in meteorite collections. However, determining the type, proportion, and amount of this material that survives atmospheric entry requires a large, unbiased, and well-preserved deposit of known age. Such a deposit has been difficult to find, given that micrometeorites generally occur in low concentrations and weather rapidly.

Here we describe micrometeorites collected from the South Pole water well (SPWW). The collection is large, well preserved, and dated; and we have previously calculated a modern-day flux for the cosmic spherule component (Taylor *et al.*, 1998). We present results primarily on cosmic spherules because unmelted micrometeorites in the samples are masked by well contaminants and are difficult to quantify. Nevertheless these results can be broadly applied. They offer information on the transformation of micrometeoroids by atmospheric entry heating, and they provide baseline data to assess effects of weathering on deposits of ancient cosmic spherules.

OTHER SAMPLE COLLECTIONS

More than a century ago, a few magnetic cosmic spherules were found in deep-sea sediments (Murray and Renard, 1891). Small numbers of cosmic spherules have subsequently been found in beach sand (Marvin and Einaudi, 1967), in swamps (Krinov, 1959), in desert sands (Fredriksson and Gowdy, 1963), in deep-sea sediments (Murrell *et al.*, 1980; Kyte, 1983; Peng and Lui, 1989), in lithified abyssal sediments (Czajkowski *et al.*, 1983; Jehanno *et al.*, 1988; Taylor and Brownlee, 1991), in Archean sandstone (Deutsch *et al.*, 1998), in polar snow and ice (Thiel and Schmidt, 1961; King and Wagstaff, 1980; Zolensky *et al.*, 1988), and in ice cores (Yiou *et al.*, 1989). The small size of these collections and the many loss mechanisms present in their various environments make it difficult to consider them unbiased representations of the spherule population.

Brownlee and coworkers analyzed the first large collection of cosmic spherules (Brownlee *et al.*, 1979; Blanchard *et al.*, 1980), obtained by sampling the top 50 cm of pelagic red clays on the Pacific Ocean floor. The depositional age of these so-called deep-sea spheres (DSS) is from recent to 0.5 Ma based on an estimated sedimentation rate of 1 m Ma^{-1}. Barred-olivine stony spherules and Fe spherules were the predominant types. Many of the stony spheres were heavily weathered, showing etched peripheries because of loss of interstitial glass.

Maurette *et al.* (1986) collected large numbers of micrometeorites from "sediment" suctioned from cryoconite holes and the bottom of melt-water streams formed on the Greenland icecap. These particles were well preserved compared to the DSS and contained many glass spherules and unmelted micrometeorites. Maurette *et al.* (1987) calculated a micrometeorite flux from the cryoconite samples, but it is subject to large uncertainties: the deposits are not closed systems and vary in particle concentration; the age of the deposits (~3000 years) and contributing ice volume were estimated from an ice-flow model.

Following success in Greenland, Maurette *et al.* (1991) obtained another large micrometeorite collection by melting 100 tons of blue ice at Cap Prudhomme (CP) on the East Antarctic plateau. An unknown process concentrates submillimeter particles just below the ice surface (Maurette *et al.*, 1994). The researchers formed large melt pockets and suctioned and sieved the water to recover ~0.15 g

Report Documentation Page

Form Approved
OMB No. 0704-0188

1. REPORT DATE	2. REPORT TYPE	3. DATES COVERED
2000		**00-00-2000 to 00-00-2000**

4. TITLE AND SUBTITLE	5a. CONTRACT NUMBER
Numbers, types, and compositions of an unbiased collection of cosmic spherules	5b. GRANT NUMBER
	5c. PROGRAM ELEMENT NUMBER
6. AUTHOR(S)	5d. PROJECT NUMBER
	5e. TASK NUMBER
	5f. WORK UNIT NUMBER
7. PERFORMING ORGANIZATION NAME(S) AND ADDRESS(ES) **U.S. Army Cold Regions Research and Engineering Laboratory,Hanover,NH,03755**	8. PERFORMING ORGANIZATION REPORT NUMBER
9. SPONSORING/MONITORING AGENCY NAME(S) AND ADDRESS(ES)	10. SPONSOR/MONITOR'S ACRONYM(S)
	11. SPONSOR/MONITOR'S REPORT NUMBER(S)

12. DISTRIBUTION/AVAILABILITY STATEMENT
Approved for public release; distribution unlimited

13. SUPPLEMENTARY NOTES
Mereonrim & PIunerury Science 35,65 1466 (2000)

14. ABSTRACT

15. SUBJECT TERMS

16. SECURITY CLASSIFICATION OF:			17. LIMITATION OF ABSTRACT	18. NUMBER OF PAGES	19a. NAME OF RESPONSIBLE PERSON
a. REPORT	b. ABSTRACT	c. THIS PAGE			
unclassified	**unclassified**	**unclassified**	**Same as Report (SAR)**	**16**	

of extraterrestrial material. These samples are rich in unmelted micrometeorites, primarily <100 μm in size. However, the age and contributing ice volume of the deposits are unknown, and no flux has been calculated.

Another rich source for micrometeorites is Antarctic surface sediment (AS) (Hagen, 1988; Koeberl and Hagen, 1989; Harvey and Maurette, 1991). These particles are found in loose sediment down wind of exposed blue ice, suggesting they are released from sublimating ice and concentrated by aeolian processes (Harvey and Maurette, 1991). Most of the micrometeorites described were partially or fully melted; there were few unmelted micrometeorites. Different degrees of weathering indicate that the spherules are of mixed depositional age (Harvey and Maurette, 1991).

Biased or poorly understood concentrating processes, uncertain depositional age, and *in situ* weathering limit the usefulness of previous collections for determining the types and numbers of micrometeorites arriving on Earth. Table 1 summarizes the principal characteristics of the largest collections.

SOUTH POLE WATER WELL COLLECTION

The SPWW provides drinking water to the Amundsen-Scott South Pole station. At the time of our deployment (1995 December), the well was 90 m below the snow surface (Fig. 1a). The pool was 24 m in diameter and 16 m deep and had melted a total of ~8000 tons of firn and ice (Taylor *et al.*, 1997). The 5000 m^3 pool melts slowly and continuously downward at a rate of ~2.4 cm/day. A pump draws water from ~3 m below the water surface. About 10% of the water is consumed, and the rest is heated and reinjected ~12 m above the well bottom. The resulting natural-convection flow is laminar, and bulk water temperatures are less than ~2 °C.

Extraterrestrial particles that fell on the snow surface became incorporated into horizontal snow–ice layers. As the well melts downward, these particles are liberated at the ice–water interface and remain on the well bottom as a concentrated lag deposit. The age of the ice melted by the SPWW is known because annual layers were counted on a nearby ice core (Kuivenan *et al.*, 1982).

We recovered micrometeorites from the SPWW using a custom-made collector. It suctioned and internally filtered the particles from the ice surface while traversing the well bottom (Fig. 1b). The collector was designed to collect all micrometeorites 50–2000 μm independent of their density, magnetic susceptibility, or shape. The average velocity through the intake slot was ~2.5× the fall velocity of a 2000 μm iron sphere, the heaviest particle of interest. We used a 50 μm polyester filter; smaller mesh sizes were considered but would have required more frequent filter changes. Particles >50 μm could not escape the collector because the filter bag was continuous, and a check valve sealed the intake slot. Laboratory tests showed that the collector's efficiency exceeded 99% on smooth or moderately rough ice (Taylor *et al.*, 1997). In the SPWW, we controlled it from the surface *via* a waterproof electromechanical cable and an underwater video system. The latter allowed us to determine the area suctioned.

At the time of deployment, the bottom of the SPWW had a gently curved central plateau (17 m^2) sculptured at its periphery into fairly steep arcuate dips that were 0.3–0.6 m below the plateau and 1–3 m wide; these dips led to smaller plateaus (2–8 m^2). Associated with most sculptured features were visibly dark pockets of particles, predominantly iron-oxide grains derived from a pump failure in the water-supply system. On the plateau areas, particles were visible but not concentrated. Local surface roughness was quite smooth (perhaps 1 mm depressions over 1 to 5 mm scales) and the ice was fracture-free. The sculptured features derive from persistent, local instabilities within the large circulation cells established by the injected water and free-convection flow along the walls (Taylor *et al.*, 1998).

We retrieved five separate samples containing a total of ~175 g of material. One deployment suctioned the central plateau, and the other deployments cleaned three adjacent pockets and their associated small plateaus. Access time and the complex bottom topography limited the collection area to 30 m^2, representing ~25% of the area with wall slopes <45°.

For each sample, we removed the polyester filter from the filter arm. We processed the plateau and one of the pocket samples in the field to assess the collector's performance. These two samples were chosen because they represent the two terrain types found on the well bottom. The remaining three samples were placed in bags, sealed, and stored for later analysis. To process a sample, we back-flushed the filter into a large high-density polyethylene (HDPE) funnel, using well water that we pressurized in a HDPE hand sprayer. The white flexible filter fabric allowed us to see particles and remove them. The sample was wet-sieved into stainless steel sieves yielding 50–106, 106–250, 250–425, and >425 μm size fractions. We estimate that cosmic spherules contstitute ~0.2 g of the 175 g recovered.

Analyses of the natural-convection flow and data obtained during collector deployment indicate that the central plateau preserves the original surface flux of micrometeorites. The depositional age of these particles was 1100–1500 A.D., and from the known area of collection, we calculated a accretion rate of 1600 ± 300 ton year^{-1} for 50–2000 μm cosmic spherules (Taylor *et al.*, 1998).

We handpicked over 1600 micrometeorites >50 μm from the plateau and pocket samples, mounted them in epoxy, sectioned them, and then sized and classified them with an optical microscope using both reflected and transmitted light. About 200 were analyzed for major elements using either the JSM-6400 at the Natural History Museum in Vienna or the JEOL35C at the University of Washington. In addition, because of the high proportion of glass spherules (relative to spherules of other textures), 169 glass spherules were analyzed with an electron microprobe at the University of Washington. Data from the energy-dispersive x-ray

TABLE 1. Principal characteristics of the different large collections.

Collection	Matrix	Mass or concentration	Age	Size range (μm)
Deep-sea spheres (DSS)	Red clays	0.1 g	<500 000 years	all
Greenland spheres (GS)	Cryoconite, meltwater	2.5×10^{-9} mg/g	~3000 years	>50
Cap Prudhomme (CP)	Ice	0.15 g	unknown	>50
Antarctic surface (AS)	Wind-blown sediment	0.2 mg/g	unknown	all
South Pole water well (SPWW)	Firn and ice	0.2 g	1100–1500 A.D.	50–2000

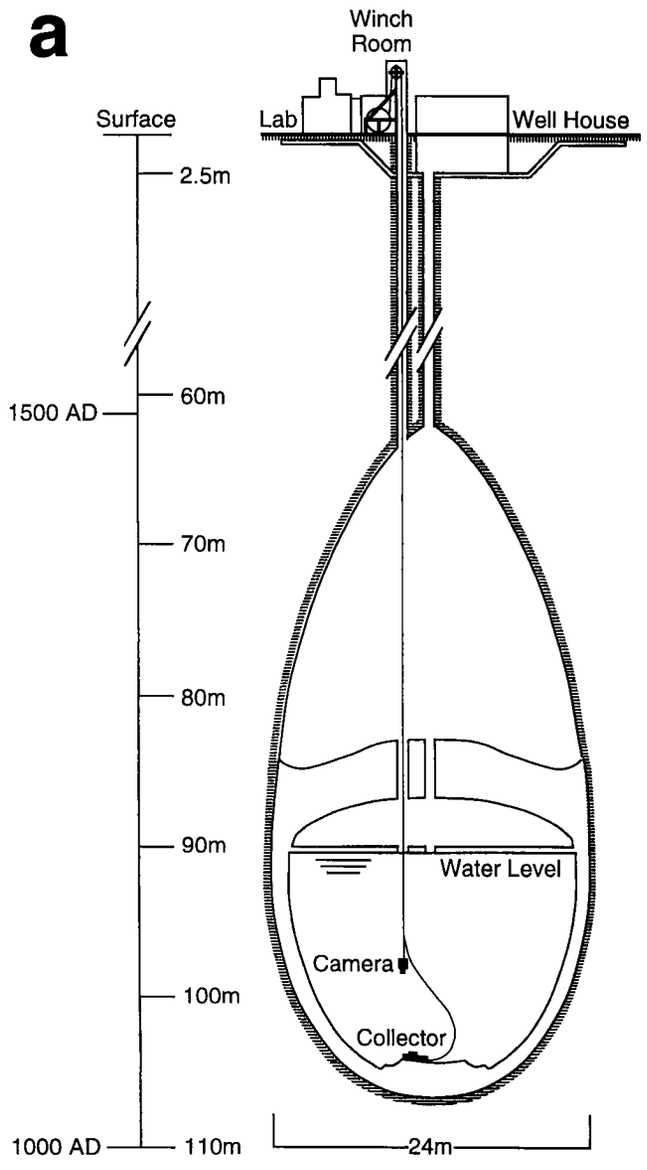

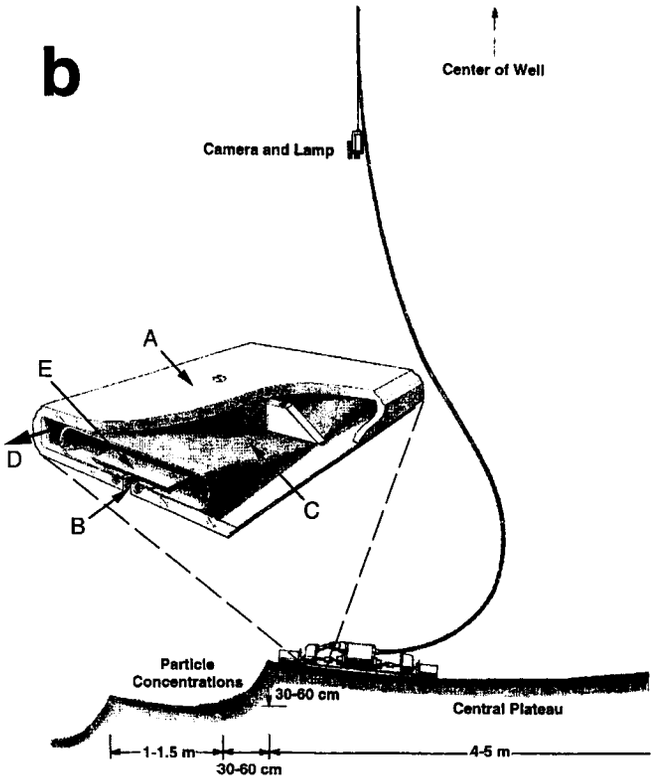

FIG. 1. (a, left) Approximate size and shape of the South Pole water well in 1995 December. (b) Schematic shows the 1.2 m long SPWW collector. The collector body (A) was made from a folded piece of low-density polyethylene. Water and particles from the ice surface are suctioned through a 2 mm slot on the bottom (B) of the collector. The water passes through a 53 μm mesh (C) and along a flow channel (D) to a pump. A plastic check-valve (E) keeps the particles in the filter.

spectrometers were quantified using an automated ZAF program along with mineral standards. A 30 μm diameter beam was used to obtain an average composition from fine-grained spherules. We used a smaller beam size to characterize the different components of particles that were not fine-grained.

PARTICLE TYPES

Extraterrestrial Components

Micrometeorites in this collection were classified into melted (cosmic spherules) and unmelted micrometeorites (irregular in shape and having magnetite rims). Descriptions and photographs of the different particle types are given below for comparison with other collections. Classes are thought to reflect both the initial composition and the heating history of the particles (Brownlee *et al.*, 1983; Taylor and Brownlee, 1991). As will be discussed, except for the I- and G-type spherules, the spherule classes are listed in order of decreasing heating.

Cosmic Spherules–Iron spherules (I-type) are composed of interlocking magnetite crystals with interstitial wüstite (Fig. 2a).

The G-type spherules have a high Fe content and contain magnetite dendrites in a glass matrix (Fig. 2b).

Stony spherules (S-type) are divided into different subclasses: CAT spherules have high Mg/Si ratios ~1.7 and more Ca, Al, and Ti than other stony spherules. They are oblate, white, and resemble barred olivine spherules but have no magnetite (Fig. 2c). Glass spherules (GL) are composed of mafic glass, are highly spherical, and sometimes have scalloped edges (Fig. 2d). Described by Maurette *et al.* (1986) and called vitreous by Robin (1988). Cryptocrystalline (CC) or glassy spherules have no visible magnetite or olivine crystals but show structure under crossed polarization (Fig. 2e). Barred olivine (BO) spherules contain lathe-shaped olivine crystals and small magnetite crystals in interstitial glass (Fig 2f); they were described by Blanchard *et al.* (1980) and called common spherules by Brownlee *et al.* (1997). Porphyritic (P) spherules have equidimensional olivine crystals and magnetite crystals in interstitial glass (Fig. 2g); they were described by Blanchard *et al.* (1980) and called equant olivine spherules by Taylor and Brownlee (1991).

Relic-grain-bearing (RGB) spherules contain relic olivine, metal, or sulfide grains within a spherule and have not been totally melted (Fig. 2h).

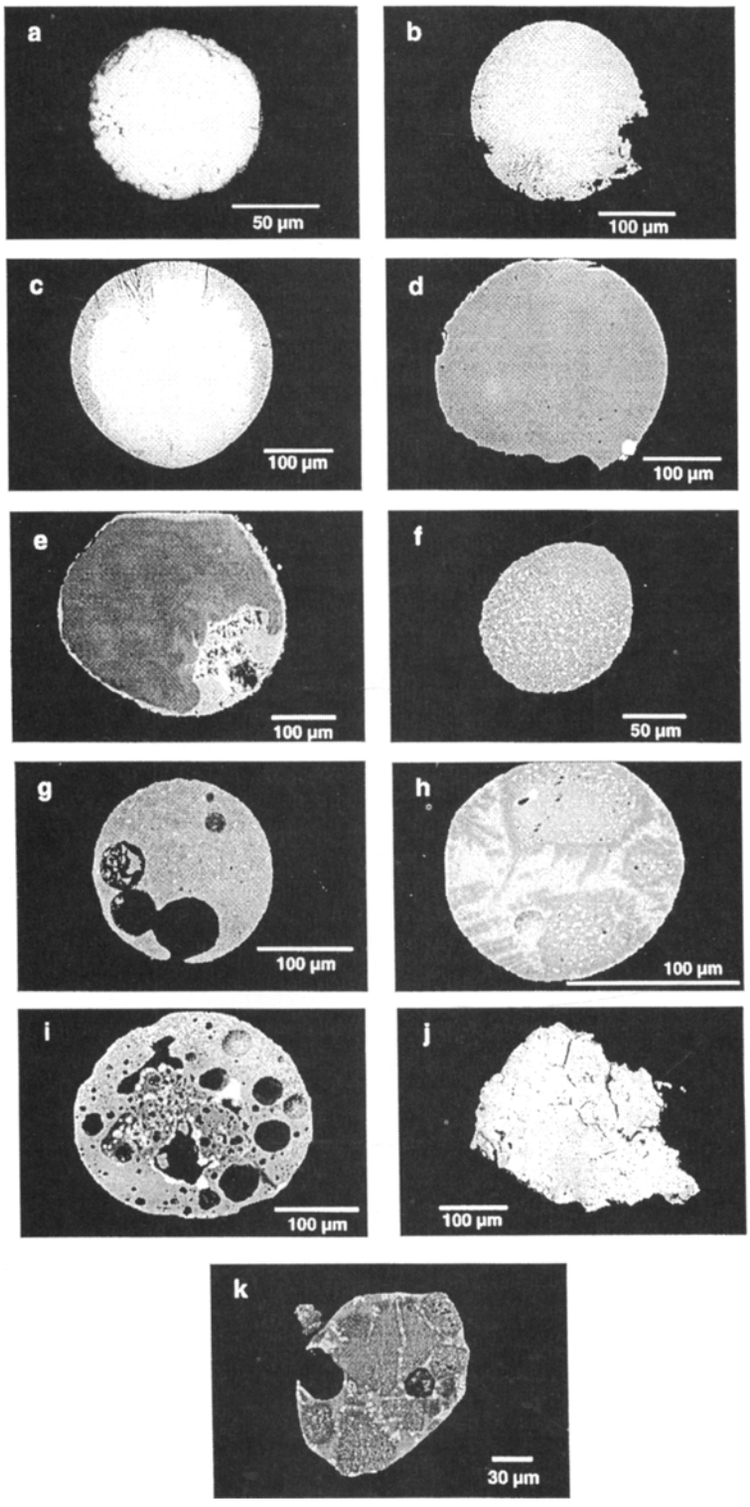

FIG. 2. Electron photomicrographs of the main classes of SPWW micrometeorites. Spherules: (a) I-type spherule; (b) G-type spherule; (c) (CAT) spherule; (d) glass spherule (GL) containing FeNi metal bead; (e) cryptocrystalline spherule (CC) with FeSNi region and coating; (f) barred olivine spherule (BO); (g) porphyritic olivine spherule (P). Partially melted: (h) relic-grain-bearing spherule (RGB) with relic forsterite grains and small distributed FeNi patches; (i) scoriaceous spherule (SC). Unmelted: (j) fine-grained (FG), IDP-like micrometeorite showing Mg-rich phyllosilicate matrix, distributed relic FeNi metal and sulfide grains, and magnetite around rim and surrounding interior voids (Note: Most of this particle is below the epoxy); (k) coarse-grained (CG) containing Fe poor pyroxene and olivines in a Fe-rich matrix.

Scoriaceous (SC) spherules are vesicular with regular or irregular cavities and contain relic olivine, metal, or sulfide grains in glass (Fig. 2i). These are transitional between unmelted and melted particles.

Unmelted Micrometeorites–Fine-grained (FG) particles are IDP-like with dark, compact matrices containing metal, sulfide, and silicate grains and chondritic composition. Magnetite rims surround the particles and most vesicles (Fig. 2j).

Coarse-grained (CG) particles containing Fe-poor pyroxenes and olivines in a Fe-rich matrix (Fig. 2k); they were described by Brownlee *et al.* (1980) and Robin *et al.* (1990).

We used the distinctive mineralogy, bulk chemistry, and internal and surface textures of our particles to identify them as micrometeorites. Measurements of cosmogenic isotopes in Fe, barred olivine, and glass spherules have proven that these particles are extraterrestrial (Nishiizumi, 1983; Raisbeck *et al.*, 1986; Nishiizumi *et al.*, 1995).

Terrestrial Weathering

The SPWW particles were immersed in pH 4.8 acidic water for <4 years, and only about half of the spherules show any signs of weathering. Unlike the DSS, the SPWW stony spherules are not etched around their periphery; rather one or two places on the margin of a sphere might have a 5–20 μm groove caused by the preferential removal of glass. As most of the interstitial glass at the margins of the SPWW spheres is still intact, we do not see the typical chatoyancy described for stony DSS (Brownlee, 1981). The high-Fe G-type and the low-Fe CAT spheres are more etched than other spherule types.

Terrestrial Components

Most of the material recovered from the well bottom is terrestrial, predominantly iron-oxide grains injected into the well from a pump failure in the water supply system (Taylor *et al.*, 1997). These grains make it difficult to find unmelted micrometeorites, which are not rounded and can look like the iron-oxide grains. Also present were wood fragments, paint chips, wire, aluminum flakes, copper spheres, and dark, nonmagnetic "glue balls". The copper spheres were injected into the well when a soldered water line in the water supply system was repaired (John Rand, pers. comm.). The "glue balls" are melted insulation formed by a fire in the pump cable in 1994 March. The contaminant spheres are easily distinguished from cosmic spherules: the copper spheres have a red or green alteration product on their surfaces, and the dark "glue balls" are soft when probed with a needle.

RESULTS

Types and Proportions of Cosmic Spherules

Table 2 shows, for each size fraction, the proportion of the samples sorted and the number of extraterrestrial particles. Of these, 1588 were sized and classified. Although the concentration of material is different on the plateau and pocket (Table 2), the size distributions for

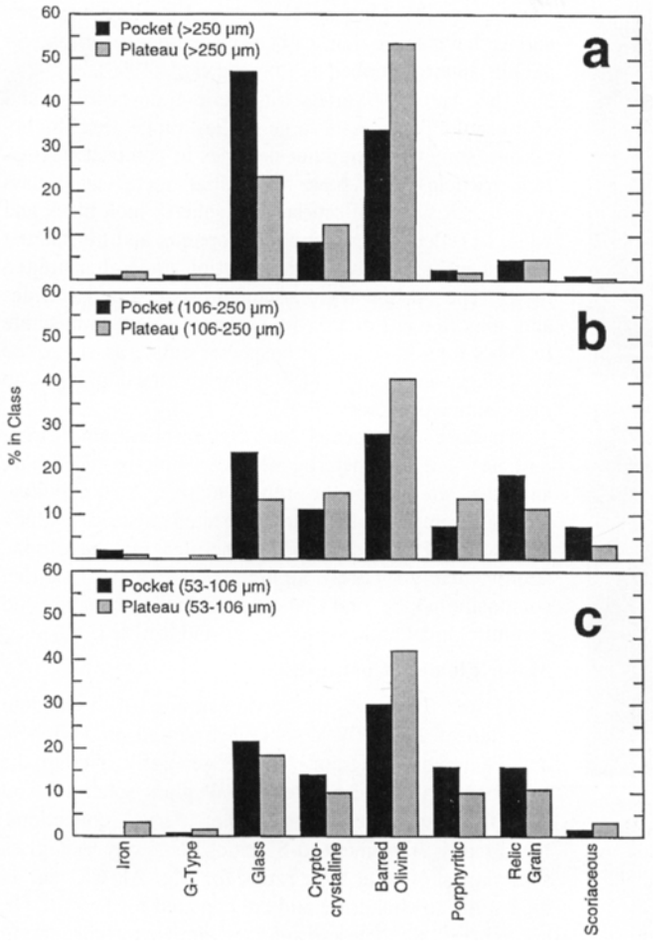

FIG. 3. Percent of particles in each of eight classes, I-type, G-type, glass, cryptocrystalline, barred olivine, porphyritic, relic grain bearing, and scoriaceous. (a) >250 μm size fraction, (b) 106–250 μm size fraction, and (c) 53–106 μm size fraction.

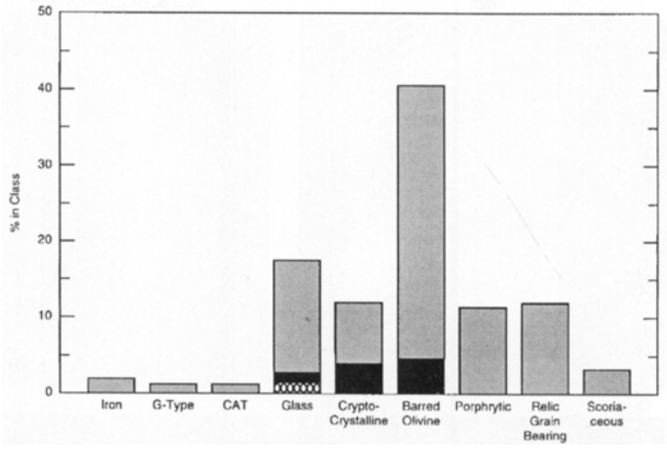

FIG. 4. Percentages of different particle types accreting to Earth based on plateau flux. The dark areas in the bars represent percent that contain metal beads; the open circles are the percent of bubble-rich glass particles.

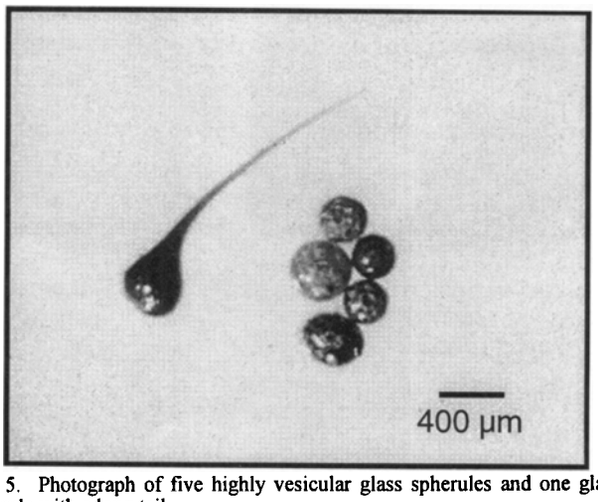

FIG. 5. Photograph of five highly vesicular glass spherules and one glass spherule with a long tail.

these two samples are identical (Taylor *et al.*, 1998). The plateau and pocket, however, have different proportions of the two most numerous spherule types, glass and barred olivine (Fig. 3). Because the particles on the plateau are derived from the ice melted directly above the plateau (Taylor *et al.*, 1998), we have used this sample to obtain the distribution of particle classes arriving on Earth.

The small size fractions contain proportionally more partially melted material (Fig. 3), and we did not sort 100% of the material <250 μm. We, therefore, normalized for the percent sorted to estimate the distribution of spherule types across all size fractions (Fig. 4). This distribution shows that 85% of cosmic spherules are totally melted and 15% are partially melted (relic-grain-bearing and scoriaceous). As has been found in other collections (Blanchard *et al.*, 1980), barred olivine spheres are the most common type. The SPWW has 41% barred olivine, 17% glass, 12% cryptocrystalline, 11% porphyritic olivine, 12% relic-grain-bearing, 3% scoriaceous, and 1% CAT spherules. The I-type and G-type constitute 2 and 1% of the spherules, respectively.

About 5% of the glass spherules are highly vesicular (Fig. 5), indicating a high volatile content. These probably weather rapidly or are easily broken, as they have not been found in other collections. Seven percent of the glass spherules, 11% of the barred olivine spherules, and 32% of cryptocrystalline spherules had one or more FeNi or FeS beads. One glass spherule contained three FeNi-metal beads. Small metal beads were mainly Ni (Fig. 2d) and may be transitional between FeNi-metal beads and Pt-group nuggets, the refractory residue of FeNi beads that are completely oxidized during atmospheric entry (Brownlee *et al.*, 1984).

Iron-nickel metal beads tend to be spherical, whereas the low surface tension of the FeS allows it to flow between the olivine crystals in the sphere. When the FeS beads intersect the surface, the sulfide coats the surface of the spherules (Fig. 2e). The surface of the spherules provides a large area from which the sulfide can evaporate. Spherules coated with iron sulfide have not been reported before, which suggests that these coatings

TABLE 2. Proportion of material examined from the SPWW.*

Sample	Plateau			Pocket		
Size range (μm)	53–106	106–250	>250	53–106	106–250	>250
Mass collected (g)	2.93	5.13	8.85	12.7	23.8	12.4
Mass examined (g)	0.248	3.50	8.85	0.349	3.62	12.4
Spherules found	122	655	183	121	731	227
Expected count	1440	960	183	4400	4810	227

*We used the number of spherules found in the mass examined to calculate the expected count (±10%).

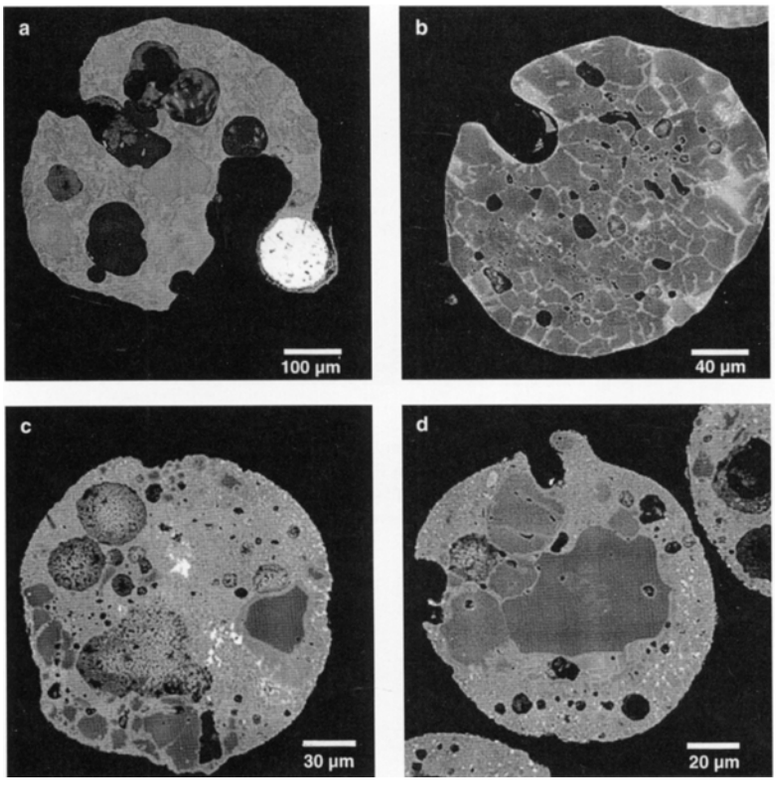

FIG. 6. Four partially melted extraterrestrial particles. (a) Bubble-rich spherule containing olivines, interstitial glass, and a large FeNiS bead. (b) Spherule composed of olivine crystals with interstitial FeS. (c) Spherule containing a forsterite relic grain and disseminated FeS. (d) Large olivine grains of different Fe contents in a fine-grained matrix of olivines, FeS, and glass.

weather rapidly. Most metal beads that intersect a sphere's surface have an Fe-rich, carbon-oxygen-phosphorus-sulfur (COPS) phase described by Engrand *et al.* (1993).

The textural variety in relic-grain-bearing and scoriaceous particles is large. They range from highly porous, somewhat irregular particles to compact olivine-rich particles that have interstitial metal and glass (Fig. 6). A subset of scoriaceous spheres look black and white in reflected light and have opaque and transparent regions when viewed in thin section under transmitted light. The opaque regions contain metals and sulfides and may have formed by separating out immiscible Fe-Ni-S liquids during atmospheric entry, as suggested by Genge and Grady (1998) for similar-looking Cap Prudhomme particles.

Because scoriaceous and some relic-grain-bearing particles are so heterogeneous, whole-particle bulk analyses would not be representative, so individual mineral compositions were collected instead. Relic grains found in the SPWW spherules include olivine (from nearly pure forsterite to more Fe-rich compositions), Fe- and Cr-bearing spinels (magnetite and chromite), pentlandite $(Fe, Ni)_9S_8$, and troilite (FeS).

Major Element Composition

Figure 7 shows the compositions of a random selection of 240 SPWW spherules plotted on a Mg, Si, and Fe ternary diagram. These generally overlap the compositional range of the SPWW glass spherules and those of spherules from other large collections. Histograms of element-to-Si ratios for stony and glass spherules show that their ratios for Mg, Al, Ca, and Ti are similar to chondritic and are depleted for Fe, Mn, Cr, and Ni (Fig. 8). These results are similar to those found

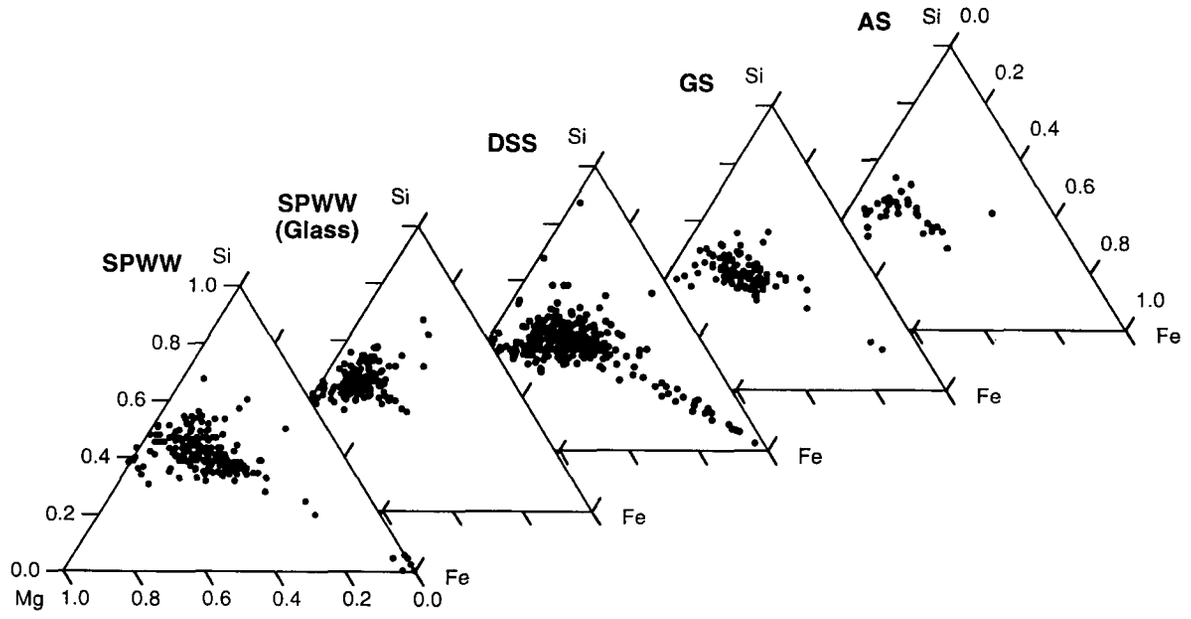

FIG. 7. Magnesium, Si, Fe (atom) ternary diagrams illustrating where SPWW spherules plot relative to other large spherule collections. (a) Energy-dispersive x-ray analyses of 240 SPWW spherules. (b) Microprobe analyses of 169 SPWW glass spherules (different particles from those shown in (a). (c) 500 deep-sea spherules plotted using data from Brownlee *et al.* (1997). (d) Greenland spherules (72 stony, 46 glass) from Robin (1988). (e) Antarctic surface spherule data (12 barred olivine, 20 glass) from Harvey and Maurette (1991).

by Brownlee *et al.* (1997) on 500 DSS spherules except for larger Fe depletion in the SPWW spherules. The DSS Fe/Si data have a broad peak centered at ~0.75 of the C1 value. Our data for stony spherules have a bimodal distribution of Fe/Si with peaks around 0.4 and 0.8 of the C1 value (Fig. 8). The glass spherules within this group are responsible for the SPWWs lower mode, and the scarcity of glass spherules in the DSS collection accounts for that collection's higher, single mode. Because data on a large number of glass spherules are not in the literature, we have included our microprobe analyses of 169 glass spherules in the appendix.

As others have noted (Blanchard *et al.*, 1980; Koeberl and Hagen, 1989; Schramm *et al.*, 1989; Brownlee *et al.*, 1997), there is a correlation between Al and Ca in micrometeorites, and both the stony and glass spherules show a trend along the solar Al/Ca line (Fig. 9). A second, less well-defined trend in Fig. 9 is consistent with particles having chondritic Al values but a range of Ca concentrations. Brownlee *et al.* (1997) suggested that meteorites with Ca-rich and Ca-poor regions reflect heterogeneity in the parent body, and dust from such bodies might produce spherules with a broad range of Ca but chondritic Al values.

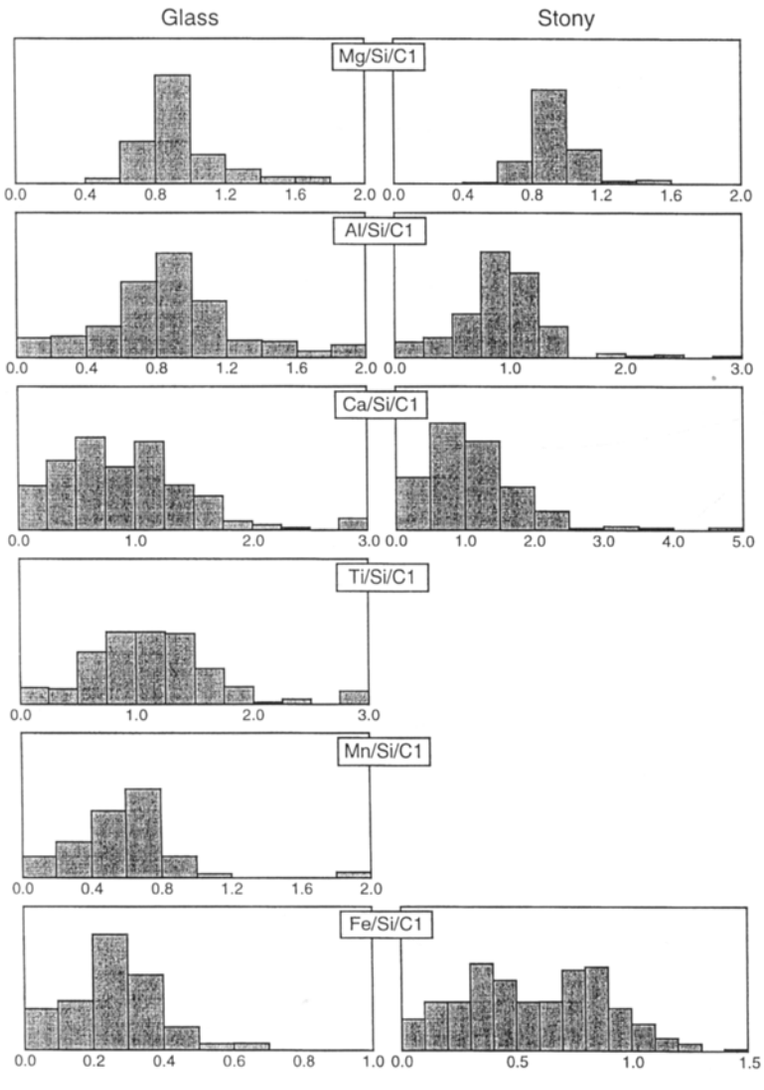

FIG. 8. Element-to-Si (atom) ratio normalized to CI for 169 glass spherules and 195 stony (all types) spherules.

Unusual Spherules

Calcium-, aluminum-, and titanium-rich (CAT) spherules had previously been reported only for the small spherules found in stratospheric collections (Brownlee *et al.*, 1982; Kordesh *et al.*, 1983). In the SPWW collection, these CAT spherules are found in all size classes, and the largest one was 325 μm in diameter. Chemical analyses of five of these spherules show that they have little Fe; have higher Ca, Al, and Ti; and a higher Mg/Si ratio than stony or glass spherules (Table 3a). The composition of these spheres is ascribed to evaporative loss of Fe and to a lesser extent of Si during atmospheric entry (Brownlee *et al.*, 1982). Oxygen-isotopic analyses on a SPWW CAT spherule found that it was highly enriched in ^{18}O, with $\delta^{18}O$ values of +40‰ as compared to +5 to +12‰ for the glass spherules (Cecile Engrand, pers. comm.). This result indicates preferential evaporation of the light isotope. Micrographs and analyses presented by Koeberl and Hagen (1989) show that their Antarctic glacial sediments also contained CAT spherules, but they were not specifically identified as such.

We also found one glass spherule that contained a pure silica phase and a two-phase metal-sulfide bead, one phase FeNi and the other FeS (Fig. 10). The shape of the dark silica phase suggests that it separated from the glass during cooling and is not a relic grain. The composition of the glass resembles that of ferrohypersthene and differs from barred olivine or glass spherules (Table 3a) in having higher Si and Mn contents and lower Mg, Ca, and Al contents. The high Mn content is unlike that found in any other spherule, and additional work is needed to determine the origin of this particle.

Unmelted Micrometeorites

Presently, we do not know the proportion of unmelted micrometeorites in the SPWW samples because of the difficulty in finding these particles among the abundant iron-oxide contaminants. Nevertheless, a variety of unmelted micrometeorites have been identified based on chondritic elemental abundance and mineral inclusions (Fig. 11). We also found unmelted micrometeorites containing framboidal magnetite (Harvey *et al.*, 1996) and one unmelted micrometeorite >700 μm across (Fig. 2j).

Maurette and his colleagues found that unmelted micrometeorites constitute 32% of their Greenland samples (Maurette *et al.*, 1987) and 40% of their Cap Prudhomme samples (Maurette *et al.*, 1991) averaged across all size fractions. Michel Maurette kindly sorted, particle by particle, a small (0.1 g) sample of the SPWW 106–250 μm size fraction. This yielded 146 cosmic spherules and 43 unmelted micrometeorites (Maurette, pers. comm.). This unmelted proportion of 23% is identical to the ratio he obtained for 100–400 μm size fraction of the CP samples (Maurette *et al.*, 1991). However, he noted that compared with the CP samples, none of SPWW unmelted micrometeorites were of the fine-grained type and that the coarse-grained ones were broken. Awoke (1998) presented analyses of some of these SPWW unmelted micrometeorites.

DISCUSSION

The SPWW collection should be an unbiased sample of the modern-day micrometeorite flux. If so, the flux, size, and composition data can help quantify the two processes that cause micrometeorites to differ from their source cosmic dust, namely atmospheric heating and terrestrial weathering. Corrected for heating effects, micrometeorites can reveal information on near-Earth cosmic dust. Corrected for weathering, ancient micrometeorite collections can provide information on the flux and composition of cosmic dust over geological time scales.

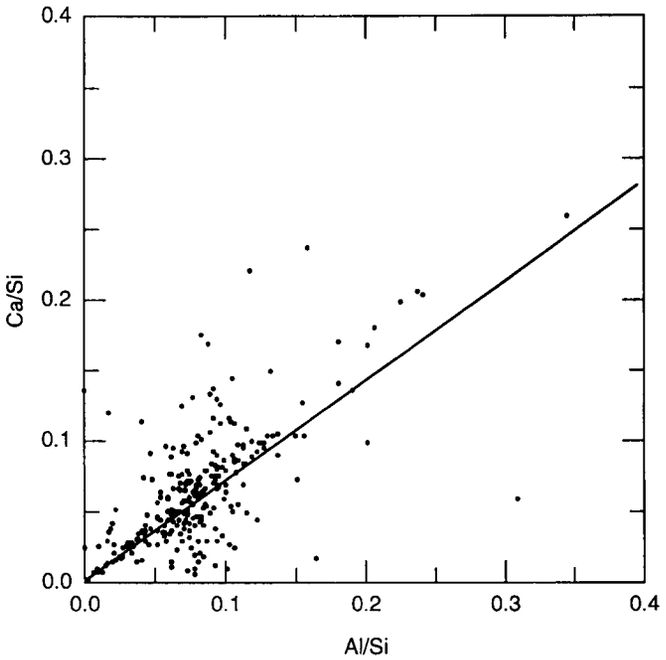

FIG. 9. Microprobe data for Ca and Al (atom), normalized to Si, are plotted for 270 glass and stony spherules relative to the solar Ca/Al ratio.

Evidence for an Unbiased Sample

The SPWW is a closed system with respect to micrometeorites. As the well melts downward, it liberates micrometeorites at the ice–water interface that then remain on the well bottom as a lag deposit. We have argued elsewhere (Taylor *et al.*, 1998) that the weak natural-convection flow field cannot entrain micrometeorites, and that the lag deposit on the SPWW central plateau preserves the original surface flux of micrometeorites. Consequently, the central plateau sample is unbiased provided that we recovered all the particles intact.

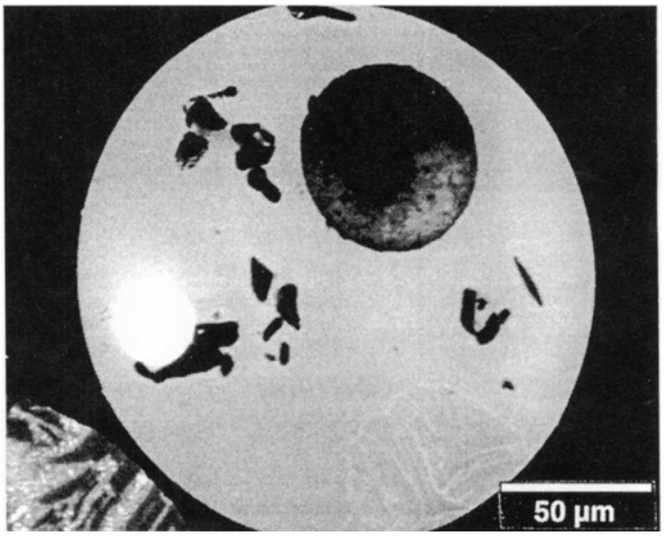

FIG. 10. Cryptocrystalline spherule containing a dark silica phase and a FeNiS bead.

TABLE 3a. Microprobe analyses of 46 barred olivine, 20 glass spherules, and 5 CAT spheres.*

Oxide	Barred olivine (x ± sd)	Glass spherules (x ± sd)	CAT spherule (x ± sd)	Glass (spherule with silica)	Olivine precursor	Pyroxene precursor
	$n = 46$	$n = 20$	$n = 5$	$n = 1$	$n = 1$	$n = 1$
MgO	26.4 ± 3.5	35.5 ± 5.0	45.7 ± 2.6	17.7	54.1	35.3
Al_2O_3	2.87± 0.8	3.42 ± 2.1	6.09 ± 1.0	1.3	1.1	1.6
SiO_2	37.5 ± 3.1	47.0 ± 3.9	41.6 ± 2.2	53.1	45.3	56.0
CaO	2.54 ± 1.1	2.97 ± 2.3	5.59 ± 1.0	1.1	0.7	1.2
TiO_2	0.13 ± 0.03	0.18 ± 0.08	0.29 ± 0.03	0.1	0.1	0.1
MnO	0.28 ± 0.1	0.27 ± 0.16	0.13 ± 0.16	3.5	0.1	0.3
FeO	26.6 ± 4.6	10.5 ± 7.5	0.95 ± 0.8	22.1	0.4	5.1
NiO	0.65 ± 0.63	0.04 ± 0.06	0.01 ± 0.01	0.1	0.0	0.0
Total	99.7 ± 0.8	100.2 ± 0.6	100.4 ± 0.6	99.0	101.8	99.6
Mount#-ID	SP-8	SP-8	SP-8,27,30	SP-30-131	SP-30-110	SP-26-28

*Also shown is the glass composition of the spherule containing the pure silica phase and two spherules that may be a melted olivine and pyroxene crystal, respectively

TABLE 3b. Comparison of element ratios of two CAT spheres with average CI composition given by Anders and Grevesse (1989).

Sample ID	Diameter (µm)	Mg/Si (atom)	Al/Si	Ca/Si	Ti/Si	Fe/Si
Bulk CI	–	1.070	0.085	0.061	0.002	0.900
Sp-8-10	300	1.71	1.910	1.350	0.005	1.00×10^{-6}
Sp-8-99	300	1.70	0.202	0.167	0.011	1.00×10^{-3}

As mentioned, the collector used in the SPWW was designed to collect all micrometeorites 50–2000 μm independent of their density, magnetic susceptibility, or shape. Laboratory tests confirmed its high collection efficiency (Taylor *et al.*, 1997). Suctioning left the SPWW plateau and nearly all of the pocket areas visibly clean, indicating high *in situ* collection efficiency based on similar laboratory results. We, therefore, conclude that the collector recovered essentially all micrometeorites present on the central plateau.

We saw no evidence of particle destruction. On the contrary, we recovered extremely delicate unmelted micrometeorites (Fig. 11), bubble-filled glass spherules, and a glass spherule with a tail whisker 5× longer than its head diameter (Fig. 5). However, the absence of FG unmelted micrometeorite in the fraction sorted by M. Maurette prompted Gounelle *et al.* (1999) to express concern that our collector could fragment the most friable, "fine-grained hydrous (FGH)" unmelted micrometeorites. Although this may be possible, we think it is unlikely. When traversing the well bottom, the collector could not crush particles because the millimeter-scale surface roughness and curvature of the well bottom prevented direct collector–particle contact. During suctioning, entrained micrometeorites traveled only a few centimeters into the collector, generally fell out of the decelerating flow before impinging on the filter mesh, and did not pass through a pump. Gounelle *et al.* (1999) also suggested that freeze-back in the SPWW could fragment FGH unmelted micrometeorites. Continuous warm-water injection and the thermal inertia of the huge SPWW ensure that the well melts continuously downward. However, freeze-back did occur following the pump failure in 1994, and this could have fragmented some fraction of the very friable FGH. Although this possibility does not affect the cosmic spherule results presented here, it warrants further consideration as we quantify the numbers and types of unmelted micrometeorites in the samples.

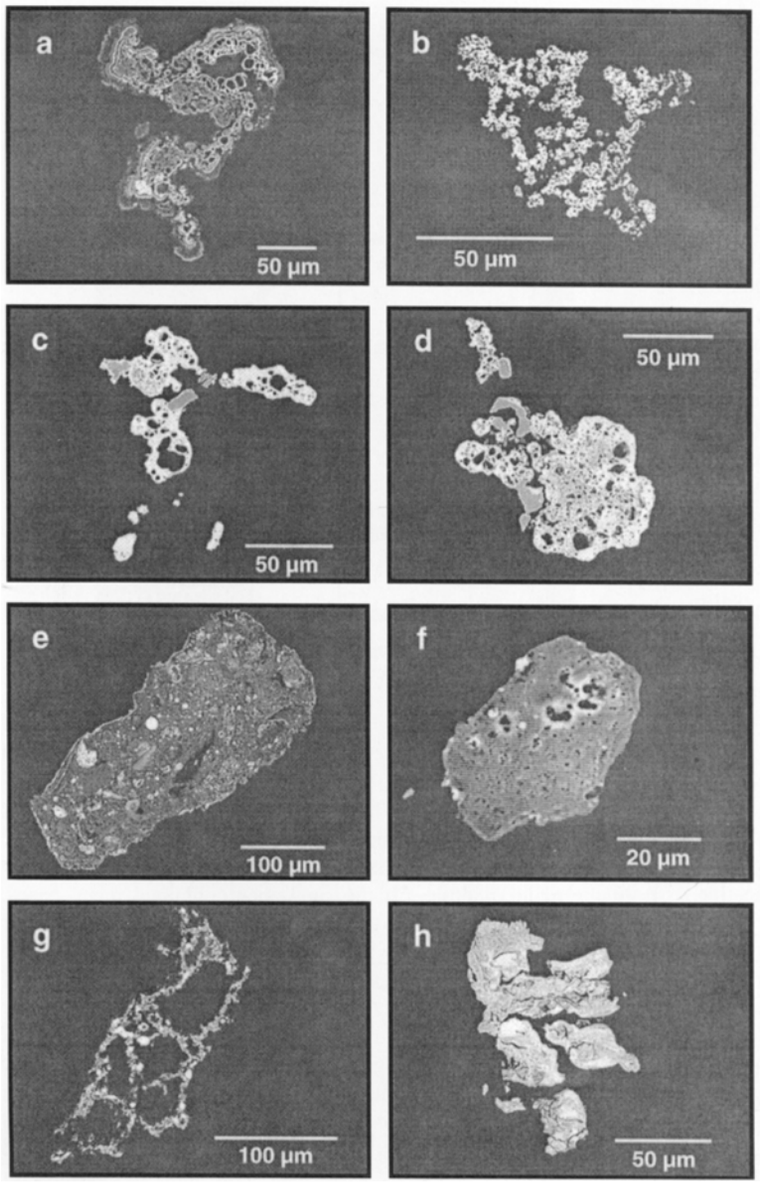

FIG. 11. Backscattered electron images of unmelted and partially melted micrometeorites from the SPWW. Bulk and spot chemistry was qualitatively determined from energy-dispersive spectra. (a) Partially melted composite particle of C-rich chondritic bulk chemistry. Concentric magnetites surround a C-rich matrix, void spaces, and the small forsteritic olivine crystals. (b) Composite particle composed primarily of FeNi metal grains and a few forsteritic olivine grains. (c) Highly distended, partially melted particle composed primarily of chondritic glass that encloses olivine crystals and vesicles. (d) Partially melted particle, containing chondritic glass and olivine crystals, whose morphology is transitional to that of a scoriaceous spherule. (e) Typical unmelted micrometeorite, consisting of olivine, pyroxene, metal and sulfide fragments in a matrix of C-rich chondritic material. Note the fine rim of magnetite along particle boundaries. (f) Another unmelted micrometeorite exhibiting diagnostic Fe enrichment around interior vesicles. (g) Highly distended particle consisting of chondritic glass, olivine, FeNi metal, and magnetite surrounding large irregular vesicles. (h) A rust particle, the main contaminant in the SPWW, is shown for comparison.

Effects of Atmospheric Heating

The SPWW collection can give the numbers, types, and sizes of cosmic dust that survives atmospheric entry. If particle classes can be linked to specific stages of heating, then models describing atmospheric heating should reproduce the number and sizes of particles in each class. Laboratory experiments help reveal this link.

The heating history of a micrometeoroid depends on its size, density, velocity, and entry angle (Flynn, 1989; Love and Brownlee, 1991). Consequently, chondritic material can yield a variety of micrometeorite classes depending on the degree and duration of heating (Brownlee *et al.*, 1983; Taylor and Brownlee, 1991; Kurat *et al.*, 1994; Greshake *et al.*, 1998). To simulate the composition changes in 50–100 μm unmelted micrometeorites, Greshake *et al.* (1998) conducted pulse-heating experiments on C1 chondritic materials. They applied heating pulses <60 s in duration and <1300 °C (*i.e.*, below the sphere-formation temperature of ~1350 °C; Love and Brownlee, 1991). They found that phyllosilicate minerals transform to olivine and pyroxenes >800 °C, whereas the elements S, Se, Ga, Ge, and Zn are lost in order from most to least volatile (Greshake *et al.*, 1998).

If micrometeorites melt fully, isothermal conditions probably exist for particles smaller than ~1000 μm (Love and Brownlee, 1991). Thus, steady-state evaporation

experiments performed by Hashimoto *et al.* (1979, 1983) using FeO-MgO-SiO_2-CaO-Al_2O_3 chondritic melts should provide insight into compositional and textural changes seen in totally melted spherules. Their experiments tracked the compositional changes in the melt residue as a function of mass loss within the temperature range 1700–2000 °C.

Their first stage of heating, defined by progressive loss of FeO, shows that the volatility sequence is FeO > SiO_2 > MgO and that CaO and Al_2O_3 are not vaporized (Hashimoto, 1983). The experimental spherules had barred olivine textures if they lost <30% of their initial mass, whereas those that lost a greater percentage had cryptocrystalline textures (Hashimoto, 1983). Although Fe loss from olivine-normative melts leads to pyroxene-normative melts, experiments have shown that the latter do not nucleate readily to form pyroxene crystals and tend to form glass when quenched (Hewins, 1983). These observations can explain barred olivine, cryptocrystalline, and glass textures and compositions seen in cosmic spherules as a sequence of increasing loss of Fe from chondritic particles. The glass spherules we observe range from dark brown, for those containing Fe/Si ratios similar to C1 chondrites, to brown, yellow, and finally colorless as their Fe content decreases. The spherules observed by Hashimoto (1983) show a similar transition of dark to light with increasing Fe loss, although they did not observe glass textures (probably because the cooling rate was too low).

Hashimoto *et al.* (1979, 1983) used thermodynamic principles to define a second stage of evaporation during which the Mg/Si ratio initially increases, because Si is more volatile, but eventually stabilizes at a Mg/Si ratio of 1.7 (olivine normative). At this point, both Mg and Si evaporate at the same rate. The CAT spherules in the SPWW could be produced by this second stage evaporation. They have Mg/Si ratios of ~1.7 (Table 3b) along with an increase in the nonvolatile species Ca, Al, and Ti.

The third and fourth stages of vaporization defined by Hashimoto *et al.* (1979, 1983) occur for mass loss exceeding ~70% and yield particles with decreasing MgO relative to SiO_2 and large proportional increases in CaO and Al_2O_3. We have not found spherules with these characteristics. Because of the severe heating needed to create them, these particles would have a very low probability of surviving atmospheric entry.

Individual spherules whose compositions do not follow the chondritic heating sequence must have derived from nonchondritic parent materials. For example, particles that lie off the solar Al/Ca line (Fig. 9) must have had starting compositions different from chondritic, because loss of Si through heating will increase the concentration but not the ratio of these elements. In addition, spherules with high Mg/Si ratios and low Fe, Ca, and Al cannot be produced by heating chondritic particles and are probably melted forsterite grains (Brownlee *et al.*, 1997). Those with low Mg/Si ratios may be a melted enstatite (Table 3a).

In addition to evaporation, buoyancy effects can be significant during atmospheric entry. Low siderophile element concentrations in stony spherules can result if FeNi-rich melts physically separate from the silicate melts (Brownlee *et al.*, 1983, 1997). In this case, Mg/Si ratios would reflect that of the parent particle. Buoyancy probably causes the physical separation, with possible density differences of 3–5 g cm^{-3} and deceleration rates that can exceed 1000 m s^{-2} (Love and Brownlee, 1991; Yada *et al.*, 1996). As mentioned, ~7% of the glass spherules, 11% of the barred olivine spherules, and 32% of cryptocrystalline spherules contain FeNi metal or FeS beads. The beads are often found near the edge of the spherule, and some spherules show evidence of having lost a metal bead.

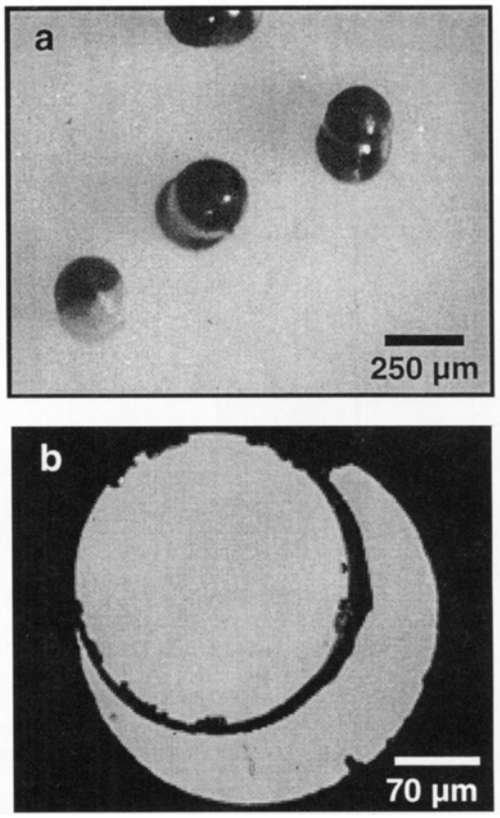

FIG. 12. Spherules with glass caps. (a) Photograph of three spherules with glass caps. (b) Micrograph of sectioned glass sphere with a glass cap.

Possibly related to the loss of metal beads are Fe-rich glass "caps" found on glass and barred olivine spherules (Fig. 12a,b). The caps range in color from white to dark brown and have pulled away from the main spherule. If the caps once contained metal beads, migration of metals towards the bead could explain the cap's higher Fe composition, and surface tension would round the cap once the bead was lost. Differential cooling might explain the separation of the cap from the spherule.

Like stony spherules, I-type spheres also show the effects of different degrees of heating. Nickel-isotopic analysis of I-type spherules from the DSS show that Ni is mass fractionated with Ni loss ranging 36–95% (Xue *et al.*, 1995). The rare, unmelted metal grains described by Maurette *et al.* (1987) may be the unmelted precursor of I-type spherules. Note that I-type spherules account for only 2% of the SPWW collection, a value similar to the 7% found for iron meteorite falls (McSween, 1987). The 30–50% I-type proportion found in the DSS collections had prompted suggestions that they are spallation products of iron meteorites; this explanation is unnecessary here.

Comparing the Effects of Terrestrial Weathering

The SPWW micrometeorites show few signs of weathering and consequently can serve as a standard to compare with other collections. In particular, we can try to address the question: Does weathering alone account for differences in spherule populations of different age and environments, or are these differences due to differences in influx or concentrating processes?

The Greenland spherules are more weathered than the SPWW spherules (Awoke, 1998) but otherwise show similar distribution of particle types (Table 4). The DSS are much more weathered (*e.g.*, missing interstitial glass) and have proportionally far fewer glass and cryptocrystalline spherules and many more I-type and G-type spherules than either polar collection (Table 4). Because the magnetically and nonmagnetically collected DSS are similar (Murrell *et al.*, 1980; Taylor and Brownlee, 1991), collection technique does not account for the paucity of glass spherules. More likely, glass-rich spherules dissolve and I-type spherules persist in deep-sea sediments (Blanchard *et al.*, 1980; Kyte, 1983). We can test this hypothesis. Dissolution of glass would essentially eliminate the glass and cryptocrystalline spherules. It would also reduce the measured accretion rate and shift the size distribution of the remaining stony spherules (BO, P, RGB, SC) because small spherules would preferentially dissolve or disaggregate. On the other hand, dissolution of glass should not affect the DSS I-type spherules and their accretion rate and size distribution should be similar to those of the SPWW.

We analyzed data from three DSS collections, described by Murrell *et al.* (1980), Kyte (1983), and Taylor and Brownlee (1991). We used SPWW data for particles >100 μm to be consistent with the particle classification comparison (Table 4) and as a median value of the smallest DSS spherules studied (50–150 μm). For SPWW cosmic spherules >100 μm, we calculate global accretion rates of 450 ± 140 ton year^{-1} for GL and CC spherules, 1000 ± 300 ton year^{-1} for stony (excluding GL and CC), and 40 ± 15 ton year^{-1} for I-type spherules.

The 0.25 m^2 DSS box core described by Taylor and Brownlee (1991) sampled the top 10–40 cm sediments. Assuming a deposition rate of 1 m Ma^{-1} for these sediments (Blanchard *et al.*, 1980) gives an age of 0.25 ± 0.15 Ma. Twenty-two of the 29 kg of the box-core sediments were processed, and 40 I-type and 49 stony spherules >100 μm were sized. The global accretion rates determined from this collection are 15 ± 10 ton year^{-1} and 35 ± 25 ton year^{-1} for I-type and stony spherules, respectively.

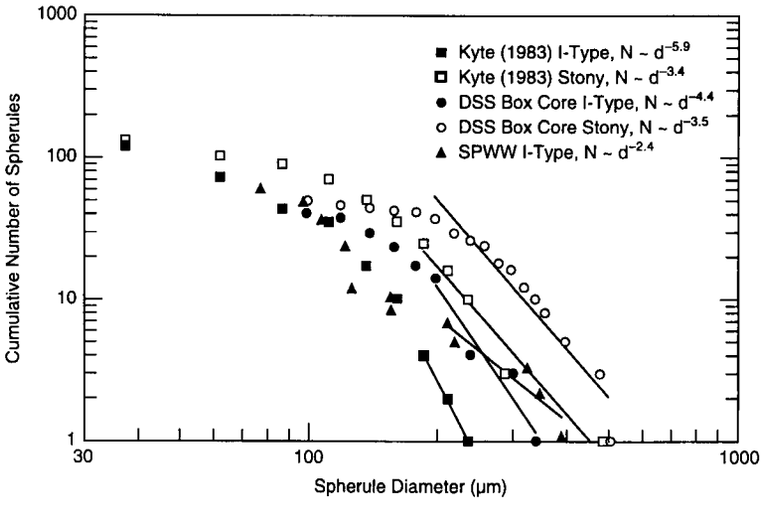

FIG. 13. Cumulative size distribution for I-type and stony spherules. The straight lines fit the distributions for diameter $d > 200$ μm using a power law $N\ (>d) \approx d^c$, with c denoting the "tail slope."

Murrell *et al.* (1980) and Kyte (1983) calculated global accretion rates of stony spherules of 90 and 370 tons year^{-1} for their respective DSS collections. Uncertainty in the sedimentation rates probably introduces ±50% uncertainty in these values. Although both groups also quantified the I-type spherules in their collections, neither reported an I-type accretion rate. From the data of Murrell *et al.* and Kyte, we cautiously estimate the accretion rates of DSS I-type spherules as 240 ± 120 and 320 ± 160 ton year^{-1}, respectively.

Figure 13 shows cumulative size distributions for stony and I-type spherules based on the SPWW and DSS box-core data and the size histograms reported by Kyte (1983). Murrell *et al.* (1980) only reported size data for stony spherules. Because of the small numbers of I-type spherules >200 μm, we estimate the uncertainties in the tail slopes of their distributions as ±50%.

Table 5 shows the stony and I-type accretion rate and size-distribution tail slopes for stony and I-type spherules for the DSS and SPWW collections. The results for stony spherules are consistent with a simple weathering hypothesis. Even with

TABLE 4. Comparison of SPWW spherule types with those >100 μm found in Antarctic aeolian deposits, Greenland, and the deep-sea collections.*

Collection	Number of spheres examined	Relic grains	Porphyritic	Barred olivine	Crypto-crystalline	Glass	G-type	Iron	Age
SPWW > 50 μm	1558	15%	11%	42%	12%	17%	1%	2%	1100–1500 A.D.
SPWW > 100 μm	1130	13%	12%	43%	15%	15%	1%	1%	same
Antarctic surface spheres (Harvey and Maurette, 1991)	?	⊢——	81%	——⊣	⊢—	18%	—⊣	–	1%	?
Greenland (Taylor and Brownlee, 1991)	92	18%	10%	55%	9%	5%	1%	1%	<3000
Greenland† (Maurette *et al.*, 1987)	667	–	–	74%	–	22%	–	4%	<3000
DSS (Taylor and Brownlee, 1991)	778	5%	9%	52%	2%	<1%	5%	26%	<500 000 (?)
DSS box core	120	6%	17%	42%	<1%	<1%	7%	27%	<500 000 (?)

*Because only particles >100 μm were classified in these former studies, we use the same lower diameter limit for the SPWW sample. For the SPWW samples, the scoriaceous spherules have been lumped with the relic-grain-bearing spherules, and the CAT spherules have been lumped with the barred olivine spherules.

†The 32% unmelted portion of the Greenland samples has been excluded and the totals recalculated.

TABLE 5. Comparison of accretion rates and slopes of cumulative size distributions for stony and I-type spherules from SPWW and three deep-sea collections.*

Collection	Stony		I-Type	
	Accretion rate (ton year^{-1})	Slope of size distribution	Accretion rate (ton year^{-1})	Slope of size distribution
Murrell *et al.* (1980)	90 ± 45†	−3.83†	240 ± 120‡	–
Kyte (1983)	370 ± 190†	−3.4 ± 0.7‡	320 ± 160‡	−5.9 ± 3.0‡
DSS Box Core	35 ± 25	−3.5 ± 0.7	15 ± 10	−4.4 ± 2.2
SPWW	1000 ± 300	−5.2 ± 0.5	40 ± 15	−2.4 ± 1.2

*Slopes are exponent, c, of best-fit power law ($N \approx d^c$) for diameter d larger than ~200 μm.
†Result reported by Murrell *et al.* (1980) or Kyte (1983) with uncertainty estimated here.
‡Result derived here based on data presented by Murrell *et al.* (1980) or Kyte (1983).

complete loss of glass and cryptocrystalline spherules from the SPWW data, the DSS stony accretion rates are lower (although they vary by order-of-magnitude) and their tail slopes are flatter (due to preferential loss of small spherules).

Results for I-type spherules are not consistent with the weathering hypothesis (*i.e.*, no differences in accretion rates and tail slopes between the DSS and SPWW collections). Allowing for large uncertainties, the I-type accretion rate and tail slope for the DSS box-core data, and the tail slope for Kyte's data, do agree with the SPWW values (Table 5). However, the I-type accretion rates calculated from the data of Murrell *et al.* and Kyte are much higher than that of the SPWW. Although both Murrell *et al.* (1980) and Kyte (1983) acknowledge that terrestrial Fe spheres could be present, Kyte found very few in his samples. More likely, their high I-type accretion rates result from poorly known sedimentation rates, unknown concentrating processes caused by ocean circulation, or a localized meteoritic event (these two sites are ~100 km apart).

CONCLUSION

The SPWW micrometeorite collection is large and unbiased with respect to cosmic spherules. The smaller unmelted component needs to be quantified to complete the description of the numbers and types of micrometeorites accreting to Earth. The collection contains the entire range of previously described cosmic spherules (I-, G-, and S-types) as well as fragile and easily weathered particles rarely seen in other collections (bubbly glasses, CAT spherules, spherules with glass caps, and ones with sulfide coatings). Also present are rare particles that have low probabilities of surviving atmospheric entry (a 700 μm unmelted micrometeorite and a spherule with a long tail). Our classification of the stony spherules is consistent with progressive evaporation of Fe from chondritic materials, and the CAT spherules appear to be an extension of this sequence. The low proportion of I-type spherules in our collection (2%) is similar to that found in Greenland and to the proportion of iron meteorite falls.

The SPWW micrometeorite collection offers a rich source of data to constrain micrometeoroid-heating models: flux and size distribution for the entire collection and for each major spherule subclass. In effect, these latter data constrain the proportion of chondritic particles heated to specific temperature intervals. This fine level of detail could help develop a micrometeoroid-heating model that accounts for the complete range of thermal transformations of incoming cosmic dust. Such a model would be a good starting point for developing an inverse transformation to give information on the size distribution and composition of the parent micrometeoroids.

Terrestrial weathering can change the size and class distributions of micrometeorites over geologic time scales. Combined with laboratory data on weathering rates for different environments, the SPWW collection can provide a baseline to assess whether the present-day micrometeorite influx can account for ancient collections (*e.g.*, from hardgrounds and Archean sandstones). Differences between the SPWW and deep-sea collections are consistent with preferential dissolution of glass and small stony spherules. However, simple weathering of the SPWW collection cannot account for the high accretion rate of I-type spherules estimated for two of the deep-sea collections. This difference could indicate changes in the composition or flux of cosmic dust over geologic time, spatial variability in the influx caused by localized events, or terrestrial concentrating processes.

Acknowledgments–We thank John Rand, John Govoni, and Michael Shandrick for their help with our fieldwork; and Dr. Cecile Engrand, Dr. Scott Kuehner, and David Josiak for help with particle analysis. We thank Dr. Michel Maurette, Dr. Gero Kurat, and Dr. T. Yada for their helpful reviews, and Dr. Donald Brownlee for his editorial handling of our paper. Collection of the micrometeorites was funded by the National Science Foundation #OPP 9316715 (Dr. Julie Palais, project manager) with additional support from CRREL. Dr. Richard Birnie and the Earth Sciences Department at Dartmouth College provided support for particle analysis through a NASA Space Grant.

Editorial handling: D. E. Brownlee

REFERENCES

ANDERS E. AND GREVESSE N. (1989) Abundances of the elements: Meteoritic and solar. *Geochim. Cosmochim. Acta* **53,** 197–214.

AWOKE V. H. (1998) Petrology, mineralogy and geochemistry of extraterrestrial dust particles from Greenland and the South Pole water well. Ph.D. thesis, Univ. Vienna, Vienna, Austria. 81 pp.

BLANCHARD M. B., BROWNLEE D. E., BUNCH T. E., HODGE P. W. AND KYTE F. T. (1980) Meteoroid ablation spheres from deep sea sediments. *Earth Planet. Sci. Lett.* **46,** 178–190.

BRADLEY J. P., SANDFORD S. A. AND WALKER R. M. (1988) Interplanetary dust particles. In *Meteorites and the Early Solar System* (eds J. F. Kerridge and M. S. Matthews), pp. 861–895. Univ. Arizona Press, Tucson, Arizona, USA.

BROWNLEE D. E. (1981) Extraterrestrial components. In *The Sea 7* (ed C. Emiliani), pp. 733–762. J. Wiley and Sons Inc., New York, New York, USA.

BROWNLEE D. E., PILACHOWSKI L. B. AND HODGE P. W. (1979) Meteorite mining on the ocean floor (abstract). *Lunar Planet. Sci.* **10,** 157–158.

BROWNLEE D. E., BATES B. A., PILACHOWSKI L. B., OLSZEWSKI E. O. and SIEGMUND W. A. (1980) Unmelted cosmic materials in deep sea sediments (abstract). *Lunar Planet Sci.* **11,** 109–111.

BROWNLEE D. E., OLSZEWSKI E. O. AND WHEELOCK M. M. (1982) A working taxonomy for micrometeorites (abstract). *Lunar Planet Sci.* **12,** 157.

BROWNLEE D. E., BATES B. A. AND BEAUCHAMPS R. H. (1983) Meteor ablation spherules as chondrule analogs. In *Chondrules and Their Origins* (ed E. A. King), pp. 10–25. Lunar and Planetary Institute, Houston, Texas, USA.

BROWNLEE D., BATES B. A. AND WHEELOCK M. M. (1984) Extraterrestrial platinum group nuggets in deep-sea sediments. *Nature* **309,** 693–695.

BROWNLEE D. E., JOSWIAK D. J. LOVE S. G., NIER A. O., SCHLUTTER D. J. AND BRADLEY J. P. (1993) Identification of cometary and asteroidal particles in stratospheric IDP collections (abstract). *Lunar Planet. Sci.* **14,** 205–206.

BROWNLEE D. E., BATES B. AND SCHRAM L. (1997) The elemental composition of stony cosmic spherules. *Meteorit. Planet. Sci.* **32,** 157–175.

CZAJKOWSKI J., ENGLERT P., BOSELLINI A. AND OGG J. G. (1983) Cobalt enriched hardgrounds—New sources of ancient extraterrestrial materials. *Meteoritics* **18,** 286–287.

DEUTSCH A., GRESHAKE A., PESONEN L. J. AND PIHLAJA P. (1998) Unaltered cosmic spherules in a 1.4-Gyr-old sandstone from Finland. *Nature* **395,** 146–148.

ENGRAND C., MAURETTE M., KURAT G., BRANDSTATTER F. AND PERREAU M. (1993) A new carbon-rich phase ("COPS") in Antarctic micrometeorites (abstract). *Lunar Planet. Sci.* **24,** 441–442.

FLYNN G. J. (1989) Atmospheric entry heating: A criterion to distinguish between asteroidal and cometary sources of interplanetary dust. *Icarus* **77,** 287–310.

FREDRIKSSON K. AND GOWDY R. (1963) Meteoritic debris from the Southern California desert. *Geochim. Cosmochim. Acta* **27,** 241–243.

GANAPATHY, R., BROWNLEE D. E. AND HODGE P. (1978) Silicate spherules from deep-sea sediments: Confirmation of extraterrestrial origin. *Science* **201,** 1119–1121.

GENGE M. J. AND GRADY M. M. (1998) Melted micrometeorites from Antarctic ice with evidence for the separation of immiscible Fe-Ni-S liquids during entry heating. *Meteorit. Planet. Sci.* **33,** 425–434.

GOUNELLE M., MAURETTE M., KURAT G. AND HAMMER C. (1999) Comparison of the 1998 "Cap-Prudhomme" and "Astrolab" Antarctic micrometeorite collections with the 1996 "South Pole" collection: Preliminary implications (abstract). *Lunar Planet. Sci.* **30,** 1564–1565.

GRESHAKE A., KLOCK W., ARNDT P., MAETZ M., FLYNN G. J., BAJT S. AND BISCHOFF A. (1998) Heating experiments simulating atmospheric entry heating of micrometeorites: Clues to their parent body sources. *Meteorit. Planet. Sci.* **33,** 267–290.

HAGEN E. H. (1988) Geochemical studies of Neogene till in the Transantarctic Mountains: Evidence for an extraterrestrial component. M.S. thesis, Ohio State University. 270 pp.

HARVEY R. P. AND MAURETTE M. (1991) The origin and significance of cosmic dust from the Walcott Névé, Antarctica. *Proc. Lunar Planet. Sci. Conf.* **21st,** 569–578.

HARVEY R. P., TAYLOR S. AND ZOLENSKY M. E. (1996) Preliminary characterization of the South Pole Water Well micrometeorites (abstract). *Meteorit. Planet. Sci.* **31 (Suppl.),** A58.

HASHIMOTO A. (1983) Evaporation metamorphism in the early solar nebula-evaporation experiments on the melt FeO-MgO-SiO_2-CaO-Al_2O_3 and chemical fractionations of primitive materials. *Geochem. J.* **17,** 111–145.

HASHIMOTO A., KUMAZAWA M. AND ONIUMA N. (1979) Evaporation metamorphism of primitive dust material in the early solar nebula. *Earth Planet. Sci. Lett.* **43,** 13–21.

HEWINS R. H. (1983) Dynamic crystallization experiments as constraints on chondrule genesis. In *Chondrules and Their Origins* (ed E. A. King). pp. 122–133. Lunar and Planetary Institute, Houston, Texas, USA.

JEHANNO C., BOCLET D., BONTE PH., CASTELLARIN A. AND ROCCHIA R. (1988) Identification of two populations of extraterrestrial particles in a Jurassic hardground of the Southern Alps. *Proc. Lunar Planet. Sci. Conf.* **18th,** 623–630.

KING E. A. AND WAGSTAFF J. (1980) Search for cometary dust in the Antarctic ice (abstract). *Antarc. J.* **15,** 78–79.

KOEBERL C. AND HAGEN E. H. (1989) Extraterrestrial spherules in glacial sediment from the Transantarctic Mountains, Antarctica; structure, mineralogy, and chemical composition. *Geochim. Cosmochim. Acta* **53,** 937–944.

KORDESH K. M., MACKINNON I. D. R. AND MCKAY D. S. (1983) A new classification and database for stratospheric dust particles (abstract). *Lunar Planet. Sci.* **14,** 389.

KRINOV E. L. (1959) Über die Natur der Mikrometeoriten. *Chem. Erde* **20,** 28–35.

KUIVINEN K. C., KOCI B. R., HOLDSWORTH G. W. AND GOW A. J. (1982) South Pole ice core drilling, 1981–1982. *Antarc. J. of the U. S.* **17,** 89–91.

KURAT G., KOEBERL C., PRESPER T., BRANDSTATTER F. AND MAURETTE M. (1994) Petrology and geochemistry of Antarctic micrometeorites. *Geochim. Cosmochim. Acta* **58,** 3879–3904.

KYTE F. T. (1983) Analyses of extraterrestrial materials in terrestrial sediments. Ph.D. thesis, University of California, Los Angeles, California, USA. 152 pp.

LOVE S. G. AND BROWNLEE D. E. (1991) Heating and thermal transformation of micrometeoroids entering the Earth's atmosphere. *Icarus* **89,** 23–46.

LOVE S. G. AND BROWNLEE D. E. (1993) A direct measurement of the terrestrial mass accretion rate of cosmic dust. *Science* **262,** 550–553.

MARVIN U. B. AND EINAUDI M. T. (1967) Black, magnetic spherules from Pleistocene and recent beach sands. *Geochim. Cosmochim. Acta* **31,** 1871–1884.

MAURETTE M., HAMMER C., BROWNLEE D. E., REEH N. AND THOMSEN H. H. (1986) Placers of cosmic dust in the blue ice lakes of Greenland. *Science* **233,** 869–872.

MAURETTE M., JEHANNO C., ROBIN E. AND HAMMER C. (1987) Characteristics and mass distribution of extraterrestrial dust from the Greenland ice cap. *Nature* **328,** 699–702.

MAURETTE M., OLINGER C., CHRISTOPHE M., KURAT G., POURCHET M., BRANDSTATTER F. AND BOUROT-DENISE M. (1991) A collection of diverse micrometeorites recovered from 100 tonnes of Antarctic blue ice. *Nature* **351,** 44–47.

MAURETTE M., HAMMMER C., HARVEY R. P., KURAT G. AND TAYLOR S. (1994) Collection and curation of IDP's in the Greenland and Antarctic ice sheets. In *Analysis of Interplanetary Dust* (ed. M. Zolensky), pp. 277–289. American Institute of Physics, Woodbury, New York, USA.

MCSWEEN H. Y., JR. (1987) *Meteorites and Their Parent Planets.* Cambridge Univ. Press, New York, New York, USA. 237 pp.

MURRELL M. T., DAVIS P. A., NISHIIZUMI K. AND MILLARD H. T. (1980) Deep-sea spherules from Pacific clay: Mass distribution and influx rate. *Geochim. Cosmochim. Acta* **44,** 2067–2074.

MURRAY J. AND RENARD A. F. (1891) *Report on the scientific results of the* H.M.S. Challenger *During the Years 1873–76,* Vol. **4** (Deep-Sea Deposits). Neill and Company, Edinburgh, Scotland. pp. 327–336.

NISHIIZUMI K. (1983) Measurement of ^{53}Mn in deep-sea iron and stonu spherules. *Earth Planet. Sci. Lett.* **63,** 223–228.

NISHIIZUMI K., ARNOLD J. R., BROWNLEE D. E., CAFFE M. W., GINKEL R. C. AND HARVEY R. P. (1995) ^{10}Be and ^{26}Al in individual cosmic spherules from Antarctica. *Meteoritics* **30,** 728–732.

PENG H. AND LUI Z. (1989) Measurement of the annual flux of cosmic dust in deep-sea sediments (abstract). *Meteoritics* **24,** 315.

PEUCKER-EHRENBRINK B. (1996) Accretion of extraterrestrial matter during the last 80 million years and its effect on the marine osmium isotope record. *Geochim. Cosmochim. Acta* **60,** 3187–3196.

PEUCKER-EHRENBRINK B. AND RAVIZZA G. (2000) The effects of sampling artifacts on cosmic dust flux estimates: A reevaluation of nonvolatile tracers (Os, Ir). *Geochim. Cosmochim. Acta* **64,** 1965–1970.

RAISBECK G. M., YIOU F., BOURLES D. AND MAURETTE M. (1986)^{10}Be and ^{26}Al in Greenland cosmic spherules: Evidence for irradiation in space as smalll objects and a probable cometary origin. *Meteoritics* **21,** 487–488.

ROBIN E. (1988) Des poussieres cosmique dans les cryoconites du Groenland: Nature, origine et applications. Ph.D. thesis, Universite de Paris-Sud, Centre D'Orsay. 131 pp.

ROBIN E., CHRISTOPHE M., BOUROT-DENISE M. AND JEHANNO C. (1990) Crystalline micrometeorites from Greenland blue lakes: Their chemical composition, mineralogy and possible origin. *Earth Planet. Sci. Lett.* **97,** 162–176.

SCHRAMM L. S., BROWNLEE D. E. AND WHEELOCK M. M. (1989) Major element composition of stratospheric micrometeorites. *Meteoritics* **24,** 99–112.

TAYLOR S. AND BROWNLEE D. E. (1991) Cosmic spherules in the geologic record. *Meteoritics* **26,** 203–211.

TAYLOR S., LEVER J. H., HARVEY R. P AND GOVONI J (1997) *Collecting Micrometeorites from the South Pole Water Well.* CRREL Report 97-1, U.S. Army Cold Regions Research and Engineering Laboratory, Hanover, New Hampshire, USA. 37 pp.

TAYLOR S., LEVER J. H. AND HARVEY R. P. (1998) Accretion rate of cosmic spherules measured at the South Pole. *Nature* **392,** 899–903.

THIEL E. AND SCHMIDT R. A. (1961) Spherules from the Antarctic ice cap. *J. Geophys. Res.* **66,** 307–310.

XUE S., HERZOG G. F., HALL G. S., BI D. AND BROWNLEE D. E. (1995) Nickel isotope abundances of I-type deep-sea spheres and of iron-nickel spherules from sediments in Alberta, Canada. *Geochem. Cosmochem. Acta* **59,** 4975–4981.

YADA T., SEKIYA M., NAKAMURA T. AND TAKAOKA N. (1996) Numerical simulation of I-type spherule formation (abstract). *Lunar Planet. Sci.* **27,** 1463–1464.

YIOU F., RAISBECK G. M. AND JEHANNO C. (1989) Influx of cosmic spherules to the Earth during the last ~10^5 years as deduced from concentrations in Antarctic ice cores (abstract). *Meteoritics* **24,** 344.

ZOLENSKY M. E., WEBB S. J. AND THOMAS K. (1988) The search for refractory interplanetary dust particles from pre-industrial aged Antarctic ice. *Proc. Lunar Plan. Sci. Conf.* **18,** 599–605.

APPENDIX

TABLE 1A. Oxide weight percent of 169 SPWW glass spherules.

Sample ID	Diameter	SiO_2	TiO_2	Al_2O_3	Cr_2O_3	FeO	MnO	NiO	MgO	CaO	Total
18-4	>425 μm	52.03	0.21	3.16	0.02	9.88	0.37	0.02	33.13	1.77	100.6
18-8		56.78	0.11	2.38	0.03	9.40	0.42	0.00	27.01	3.80	99.9
18-13a		45.82	0.19	4.14	0.14	10.03	0.15	0.03	35.46	3.69	99.7
18-5		47.50	0.13	2.91	0.12	14.20	0.89	0.26	31.03	2.52	99.6
18-7		48.75	0.60	14.31	0.02	15.70	0.45	0.00	7.08	11.76	98.7
28-1	>425 μm	41.93	0.22	4.92	0.02	13.69	0.17	0.00	35.95	3.47	100.4
28-2		51.08	0.17	3.34	0.17	10.01	0.38	0.00	33.33	1.10	99.6
28-5		54.36	0.14	1.93	0.07	9.83	0.36	0.06	27.31	5.69	99.8
28-30		48.38	0.18	3.90	0.02	13.00	0.38	0.00	29.61	3.58	99.1
28-31		47.62	0.10	3.39	0.04	15.06	0.31	0.18	31.14	1.90	99.7
28-29		55.49	0.19	2.05	0.08	12.42	0.34	0.01	24.78	3.80	99.2
28-28		51.14	0.15	3.26	0.19	14.44	0.39	0.00	26.58	3.32	99.5
28-27		50.87	0.13	2.80	0.04	11.46	0.37	0.03	28.86	4.48	99.0
28-24		52.32	0.24	2.79	0.19	15.94	0.33	0.00	23.14	4.31	99.3
28-23		46.21	0.16	3.75	0.00	7.27	0.23	0.08	38.51	3.83	100.0
28-22		55.96	0.18	3.52	0.35	9.99	0.36	0.03	25.81	2.97	99.2
28-15		47.22	0.07	2.71	0.04	17.41	0.34	0.00	28.42	3.27	99.5
28-12		46.81	0.13	2.54	0.20	15.87	0.41	0.08	31.61	1.85	99.5
28-11		45.55	0.08	2.62	0.00	10.95	0.38	0.01	38.09	2.77	100.5
28-9		51.94	0.47	13.68	0.00	11.00	0.20	0.00	19.28	2.81	99.4
29-1	250–425 μm	52.72	0.13	2.49	0.01	10.09	0.46	0.02	32.32	2.12	100.4
29-2		44.35	0.19	4.62	0.01	13.05	0.19	0.02	35.25	1.77	99.5
29-3		49.91	0.15	3.11	0.02	15.39	0.37	0.04	29.02	2.04	100.0
29-44		49.25	0.11	3.44	0.02	18.68	0.40	0.24	26.39	2.10	100.6
29-45		49.08	0.69	10.10	0.32	20.94	0.65	0.01	8.45	9.27	99.5
29-6		42.45	0.23	5.45	0.00	8.61	0.13	0.00	39.66	4.05	100.6
29-7		53.11	0.11	3.06	0.20	10.12	0.41	0.00	30.93	2.12	100.1
29-48		47.17	0.25	5.23	0.05	12.44	0.20	0.00	30.11	4.54	100.0
29-49		56.68	0.11	2.29	0.12	12.52	0.44	0.14	21.92	4.78	99.0
29-9		50.17	0.11	3.36	0.03	17.10	0.29	0.37	26.63	1.84	99.9
29-51		47.69	1.10	0.76	0.00	29.99	1.07	0.01	14.18	5.29	100.1
29-54		46.77	0.17	2.78	0.00	6.68	0.22	0.00	37.25	5.36	99.2
29-11		48.71	0.22	5.31	0.15	8.54	0.15	0.05	32.67	4.45	100.2
29-56		40.95	0.16	3.46	0.06	24.28	0.26	0.07	28.26	3.28	100.8
29-13		51.16	0.17	3.15	0.14	15.24	0.12	0.00	27.57	3.06	100.6
29-14		50.91	0.15	3.47	0.06	11.43	0.33	0.05	28.11	4.61	99.1
29-59		53.92	0.16	2.43	0.10	10.20	0.51	0.04	32.36	1.28	101.0
29-68		48.25	0.14	3.48	0.26	17.44	0.37	0.08	27.82	2.33	100.2
29-67		47.98	0.06	1.82	0.18	15.87	0.50	0.03	32.44	1.42	100.3
29-60a		47.33	0.10	2.80	0.03	14.60	0.31	0.00	32.14	2.81	100.1
29-61		54.60	0.24	3.91	0.08	10.77	0.31	0.06	21.40	8.85	100.2
29-62		50.16	0.09	1.90	0.43	16.07	0.45	0.07	29.23	1.33	99.7
29-66a		49.71	0.13	3.40	0.30	10.74	0.50	0.00	32.71	2.93	100.4
29-21		43.40	0.15	3.12	0.01	16.76	0.35	0.00	33.22	2.61	99.6
29-63		47.61	0.16	3.41	0.42	14.95	0.46	0.00	30.43	2.79	100.2
29-65		47.52	0.14	2.38	0.11	15.28	0.38	0.28	33.03	1.26	100.4
29-69		53.20	0.19	2.03	0.04	15.08	0.42	0.00	27.21	1.80	100.0
29-70		47.89	0.09	2.57	0.06	14.88	0.38	0.08	32.15	2.23	100.3
29-23		44.48	0.17	3.58	0.10	18.35	0.31	0.00	29.72	2.84	99.6
29-25		48.17	0.15	3.91	0.04	11.34	0.30	0.02	33.37	3.02	100.3
29-30		45.14	0.12	2.63	0.03	16.64	0.31	0.52	32.85	1.39	99.6
29-31		46.29	0.11	2.40	0.32	23.20	0.38	0.02	25.89	2.15	100.8
29-32		51.05	0.09	0.85	0.54	9.86	0.56	0.07	35.50	1.76	100.3
29-35		53.99	0.09	2.54	0.05	13.25	0.51	0.10	25.85	3.15	99.5
29-37		49.30	0.13	3.30	0.02	1.76	0.00	0.00	43.06	2.78	100.4
29-40		48.46	0.15	3.01	0.09	12.00	0.45	0.01	33.09	3.15	100.4
29-41		41.74	0.17	4.90	0.02	12.61	0.12	0.00	36.27	4.05	99.9
29-42		58.62	0.00	0.15	0.33	14.79	0.25	0.04	25.58	0.09	99.9
29-43		46.78	0.22	2.38	0.03	11.03	0.09	0.00	37.81	2.58	100.9

TABLE 1A. *Continued.*

Sample ID	Diameter	SiO_2	TiO_2	Al_2O_3	Cr_2O_3	FeO	MnO	NiO	MgO	CaO	Total
15-46	250–425 μm	49.01	0.16	3.01	0.06	11.63	0.46	0.00	34.56	2.58	101.5
15-47		49.96	0.18	3.29	0.21	9.42	0.35	0.00	34.24	2.09	99.7
15-49		55.81	0.15	3.15	0.13	13.60	0.42	0.04	25.66	1.18	100.1
15-24		43.66	0.15	1.54	0.03	17.95	0.33	0.03	32.39	1.41	97.5
15-26		47.42	0.11	2.86	0.08	17.22	0.34	0.00	30.36	2.16	100.6
15-50		53.98	0.20	3.91	0.07	7.79	0.49	0.06	31.03	3.19	100.7
15-28		49.20	0.16	3.12	0.13	16.24	0.33	0.02	29.65	1.64	100.5
15-27		49.76	0.12	2.66	0.02	13.66	0.39	0.01	31.45	1.68	99.7
15-29		41.07	0.10	2.99	0.00	3.34	0.22	0.00	35.45	18.14	101.3
15-30		42.06	0.26	5.44	0.00	4.71	0.06	0.00	45.23	2.82	100.6
15-31		52.79	0.09	1.04	0.20	2.86	0.27	0.04	42.88	0.74	100.9
15-32		41.98	0.17	3.88	0.01	16.98	0.19	0.00	34.44	3.02	100.7
15-33		47.60	0.12	2.86	0.20	21.12	0.31	0.02	26.86	1.29	100.4
15-34		42.17	0.21	3.60	0.01	21.49	0.23	0.03	29.93	2.47	100.1
15-35		42.82	0.29	6.04	0.00	4.59	0.11	0.00	46.15	0.66	100.7
15-36		44.83	0.17	3.89	0.25	20.16	0.19	0.38	30.88	0.35	101.1
24-2	250–425 μm	48.96	0.15	2.56	0.11	16.54	0.41	0.00	27.88	3.46	100.1
24-3		49.14	0.12	2.52	0.19	16.46	0.41	0.00	28.86	1.99	99.7
24-8		45.16	0.11	3.07	0.13	22.37	0.24	0.53	26.71	2.74	101.1
24-11		51.52	0.22	2.63	0.30	20.49	0.38	0.05	22.40	2.77	100.8
24-16		55.25	0.14	3.33	0.24	9.52	0.38	0.01	25.74	4.87	99.5
24-26		41.69	0.16	3.48	0.00	20.80	0.36	0.02	30.33	3.10	99.9
24-33		42.60	0.20	4.10	0.00	13.80	0.26	0.15	34.78	3.84	99.8
24-47		50.38	0.01	0.16	0.20	14.64	2.39	0.05	32.35	0.09	100.3
24-43		46.03	0.12	2.51	0.35	15.18	0.34	0.01	35.13	2.07	101.7
24-45		48.69	0.05	0.85	0.19	14.51	0.62	0.01	34.42	0.62	100.0
24-52		45.23	0.11	3.03	0.39	18.67	0.52	0.14	29.79	2.73	100.6
24-56		45.20	0.15	3.24	0.03	16.34	0.30	0.00	30.79	4.19	100.2
24-68		49.47	0.19	2.50	0.25	18.98	0.30	0.01	24.30	4.39	100.4
24-73		47.76	0.18	3.72	0.39	14.01	0.36	0.00	30.47	3.27	100.2
24-79		46.81	0.19	3.87	0.14	20.86	0.53	0.36	19.11	4.87	96.7
24-89		41.09	0.10	2.77	0.68	28.83	0.17	0.03	26.68	0.71	101.1
24-90		42.32	0.19	3.73	0.00	20.13	0.26	0.00	32.74	1.02	100.4
24-114		48.18	0.09	0.93	0.03	15.71	0.27	0.18	33.40	1.15	100.0
24-115		50.35	0.19	2.27	0.11	10.84	0.18	0.11	35.88	1.25	101.2
24-121		39.56	0.13	3.15	0.05	30.67	0.24	0.03	25.62	1.38	100.8
30-0	106–250 μm	40.18	0.25	6.18	0.02	9.82	0.12	0.00	38.63	5.25	100.4
30-1		40.44	0.11	2.92	0.61	28.30	0.38	0.08	26.70	1.52	101.1
30-2		46.50	0.09	2.49	0.39	16.17	0.46	0.02	31.95	2.02	100.1
30-3		54.08	0.09	1.54	0.08	7.43	0.52	0.04	34.17	1.36	99.3
30-4		52.86	0.07	4.13	0.52	10.61	0.56	0.05	25.82	5.67	100.3
30-12		47.10	0.14	3.11	0.02	11.46	0.37	0.17	34.55	2.76	99.7
30-14		55.37	0.13	2.72	0.23	11.88	0.54	0.00	27.41	1.76	100.0
30-24		44.08	0.16	2.86	0.15	20.24	0.29	0.02	29.16	2.90	99.9
30-27		52.31	0.12	1.70	0.79	11.24	0.38	0.03	32.21	1.46	100.2
30-33		43.94	0.05	2.77	0.00	18.12	0.36	0.12	30.44	3.70	99.5
30-34		40.80	0.01	0.58	0.03	28.27	0.47	0.02	29.99	0.48	100.7
30-36		34.93	0.12	2.31	0.33	36.00	0.23	0.59	23.97	1.76	100.2
30-38		46.92	0.10	4.53	0.11	18.47	0.31	0.77	22.68	3.65	97.5
30-40		47.50	0.00	0.28	0.08	18.12	0.40	0.05	32.84	0.27	99.5
30-53		45.92	0.12	2.45	0.10	19.12	0.43	0.02	29.67	1.53	99.4
30-54		49.76	0.06	0.69	0.29	14.37	0.55	0.00	33.72	0.55	100.0
30-60		48.51	0.13	3.06	0.03	13.62	0.35	0.00	31.05	2.32	99.1
30-61		44.94	0.11	3.25	0.04	18.59	0.18	0.01	31.54	0.75	99.4
30-66		50.57	0.06	0.59	0.00	12.01	0.92	0.00	35.03	0.27	99.4
30-67		48.31	0.09	2.20	0.02	9.13	0.22	0.03	37.43	1.99	99.4
30-75		48.69	0.16	3.01	0.55	16.85	0.46	0.03	27.67	2.61	100.0
30-82		48.09	0.07	1.46	0.02	14.51	0.79	0.25	32.15	1.08	98.4
30-88		45.40	0.13	2.22	0.01	22.13	0.37	0.04	27.30	1.35	99.0
30-91		46.12	0.13	3.07	0.12	18.80	0.26	0.28	29.40	0.40	98.6
30-92		51.27	0.03	0.41	0.01	12.12	1.28	0.03	33.87	0.30	99.3
30-93		36.09	0.08	1.92	0.59	33.66	0.44	0.00	24.65	1.72	99.2
30-94		47.92	0.14	3.34	0.11	13.62	0.40	0.00	30.80	3.04	99.4

TABLE 1A. *Continued.*

Sample ID	Diameter	SiO_2	TiO_2	Al_2O_3	Cr_2O_3	FeO	MnO	NiO	MgO	CaO	Total
30-97	106–250 μm	48.95	0.06	1.66	0.02	14.09	0.72	0.02	33.11	1.37	100.0
30-98		51.57	0.16	4.25	0.02	12.65	0.34	0.04	25.85	6.02	100.9
30-101		49.97	0.08	2.48	0.07	13.54	0.37	0.00	32.11	1.63	100.3
30-103		46.27	0.05	1.63	0.00	14.79	0.49	0.03	36.31	0.66	100.2
30-108		47.83	0.19	3.89	0.03	9.49	0.21	0.02	35.65	3.30	100.6
30-115		41.44	0.19	4.55	0.02	13.70	0.15	0.00	36.45	3.65	100.1
30-116		45.50	0.08	1.64	0.20	19.33	0.37	0.19	30.88	1.54	99.7
30-130		48.16	0.16	2.54	0.36	16.35	0.37	0.01	30.33	1.51	99.8
30-131		53.09	0.06	1.26	0.61	22.09	3.53	0.08	17.70	1.13	99.6
30-137		48.16	0.21	4.46	0.00	13.02	0.38	0.00	30.30	3.84	100.4
30-139		44.49	0.21	4.70	0.01	7.43	0.18	0.01	39.21	4.06	100.3
30-143		53.76	0.16	2.63	0.28	14.10	0.43	0.06	25.14	1.99	98.6
30-153		60.53	0.10	2.00	0.03	5.43	0.19	0.10	29.96	1.89	100.2
30-152		51.97	0.14	2.78	0.09	13.01	0.42	0.02	30.53	0.64	99.6
27-1	106–250 μm	54.86	0.19	4.48	0.00	5.46	0.57	0.01	32.47	3.40	101.4
27-2		47.51	0.13	3.00	0.54	19.53	0.31	0.02	28.03	0.33	99.4
27-3		48.21	0.14	3.51	0.41	18.18	0.28	0.02	26.33	2.96	100.1
27-4		56.97	0.16	0.53	0.12	10.55	0.43	0.00	30.17	1.34	100.3
27-5		49.05	0.23	4.51	0.27	11.20	0.22	0.01	30.56	3.96	100.0
27-6		44.41	0.15	2.00	0.00	1.63	0.05	0.03	51.32	1.46	101.1
27-7		50.32	0.09	1.46	0.01	0.48	0.09	0.01	47.92	1.29	101.7
27-8		50.55	0.14	3.16	0.71	11.35	0.38	0.00	30.76	2.70	99.8
27-9		49.20	0.15	2.73	0.01	3.52	0.11	0.00	42.79	2.22	100.7
27-10		43.86	0.02	0.38	0.01	0.49	0.00	0.02	55.66	0.35	100.8
27-11		54.91	0.16	4.59	0.00	13.37	0.29	0.02	24.95	1.66	100.0
27-12		45.10	0.18	3.87	0.10	3.26	0.18	0.09	44.43	3.27	100.5
27-13		43.30	0.07	2.75	0.00	2.97	0.04	0.03	49.51	1.63	100.3
27-14		44.94	0.21	4.68	0.00	4.50	0.27	0.00	41.52	3.84	100.0
27-15		47.95	0.17	3.81	0.03	10.10	0.40	0.02	33.43	3.21	99.1
27-16		41.38	0.33	7.26	0.01	1.29	0.02	0.00	42.55	6.91	99.8
27-17		42.13	0.00	2.90	0.02	0.01	0.00	0.01	54.21	0.54	99.8
27-18		55.11	0.15	3.49	0.11	13.61	0.40	0.16	24.57	1.61	99.2
34-13	53–106 μm	46.34	0.19	4.33	0.64	14.34	0.33	0.00	31.01	3.67	100.9
34-15		43.87	0.14	2.93	0.69	25.06	0.22	0.00	27.03	0.22	100.2
34-12		48.50	0.15	2.92	0.02	12.24	0.61	0.01	32.03	2.53	99.0
34-21		39.94	0.14	3.20	0.17	28.71	0.25	0.05	27.04	1.06	100.6
34-25		43.39	0.07	0.80	0.00	0.07	0.01	0.06	55.01	0.79	100.2
34-30		45.88	0.18	3.22	0.01	13.66	0.34	0.00	34.33	2.62	100.2
34-42		42.14	0.08	2.38	0.08	18.48	0.43	0.39	35.33	1.57	100.9
34-43		40.00	0.09	2.14	0.27	16.61	0.22	0.32	40.87	0.36	100.9
34-57		43.34	0.14	3.40	0.00	0.01	0.00	0.00	51.71	2.08	100.7
34-56		45.48	0.15	3.37	0.13	22.25	0.31	0.69	23.99	3.29	99.7
34-65		48.87	0.18	3.39	0.21	11.68	0.18	0.00	33.86	1.32	99.7
34-86		41.09	0.12	2.64	0.11	26.49	1.27	0.10	26.66	2.29	100.8
34-85		44.95	0.15	2.13	0.34	20.12	0.32	0.55	29.82	2.49	100.9
34-84		50.97	0.19	4.00	0.00	1.17	0.31	0.00	40.45	3.27	100.4
34-83		48.91	0.08	1.06	0.72	10.88	0.93	0.02	34.13	0.79	97.5
34-0		49.92	0.15	2.65	0.11	16.25	0.35	0.01	27.24	3.54	100.2
Average		47.87	0.15	3.10	0.14	14.03	0.38	0.07	31.63	2.64	100.0
Std. Dev.		4.5	0.1	1.8	0.2	6.5	0.3	0.1	7.2	2.1	0.8